

**Regional climate
model simulations for
Europe at 6 k and
0.2 kyr BP**

G. Strandberg et al.

Regional climate model simulations for Europe at 6 k and 0.2 kyr BP: sensitivity to changes in anthropogenic deforestation

G. Strandberg^{1,2}, E. Kjellström^{1,2}, A. Poska^{3,5}, S. Wagner⁴, M.-J. Gaillard⁵, A.-K. Trondman⁵, A. Mauri⁶, H. J. B. Birks^{7,8,9}, A. E. Bjune¹⁰, B. A. S. Davis⁶, R. Fyfe¹¹, T. Giesecke¹², L. Kalnina¹³, M. Kangur¹⁴, J. O. Kaplan⁶, W. O. van der Knaap¹⁵, U. Kokfelt^{16,3,5}, P. Kuneš¹⁷, M. Latałowa¹⁸, L. Marquer⁵, F. Mazier^{19,3}, A. B. Nielsen^{20,5}, B. Smith³, H. Seppä²¹, and S. Sugita¹⁴

¹Swedish Meteorological and Hydrological Institute, Norrköping, Sweden

²Department of Meteorology, Stockholm University, Stockholm, Sweden

³Department of Earth and Ecosystem Science, Lund University, Lund, Sweden

⁴Helmholtz-Zentrum Geesthacht, Geesthacht, Germany

⁵Department of Biology and Environmental Science, Linnaeus University, Kalmar, Sweden

⁶ARVE, École polytechnique fédérale de Lausanne, EPFL, Lausanne, Switzerland

⁷Department of Biology and Bjerknes Centre for Climate Research University of Bergen, Bergen, Norway

⁸Environmental Change Research Centre, University College London, London, UK

⁹School of Geography and the Environment, University of Oxford, Oxford, UK

Title Page

Abstract

Introduction

Conclusions

References

Tables

Figures

⏪

⏩

◀

▶

Back

Close

Full Screen / Esc

Printer-friendly Version

Interactive Discussion

Regional climate model simulations for Europe at 6 k and 0.2 kyr BP

G. Strandberg et al.

Title Page

Abstract

Introduction

Conclusions

References

Tables

Figures

⏪

⏩

◀

▶

Back

Close

Full Screen / Esc

Printer-friendly Version

Interactive Discussion

¹⁰Uni Climate, Uni Research AS and Bjerknes Centre for Climate Research, Bergen, Norway

¹¹School of Geography, Earth and Environmental Sciences, University of Plymouth, Plymouth, UK

¹²Department of Palynology and Climate Dynamics, Albrecht-von-Haller-Institute for Plant Sciences, University of Göttingen, Göttingen, Germany

¹³Faculty of Geography and Earth Sciences, University of Latvia, Riga, Latvia

¹⁴Institute of Ecology, Tallin University, Tallin, Estonia

¹⁵Institute of Plant Sciences and Oeschger Centre for Climate Change Research, University of Bern, Bern, Switzerland

¹⁶Center for Permafrost, Department of Geosciences and Natural Resource Management, University of Copenhagen, Copenhagen, Denmark

¹⁷Department of Botany, Faculty of Science, Charles University in Prague, Praha, Czech Republic

¹⁸Laboratory of Palaeoecology and Archaeobotany, Department of Plant Ecology, University of Gdańsk, Gdańsk, Poland

¹⁹GEODE, UMR5602, University of Toulouse, Toulouse, France

²⁰Department of Geology, Lund University, Lund, Sweden

²¹Department of Geosciences and Geography, University of Helsinki, Helsinki, Finland

Received: 30 September 2013 – Accepted: 7 October 2013 – Published: 18 October 2013

Correspondence to: G. Strandberg (gustav.strandberg@smhi.se)

Published by Copernicus Publications on behalf of the European Geosciences Union.

Abstract

This study aims to evaluate the direct effects of anthropogenic deforestation on simulated climate at two contrasting periods in the Holocene, ~ 6 kBP and ~ 0.2 kBP in Europe. We apply RCA3, a regional climate model with 50 km spatial resolution, for both time periods, considering three alternative descriptions of the past vegetation: (i) potential natural vegetation (V) simulated by the dynamic vegetation model LPJ-GUESS, (ii) potential vegetation with anthropogenic land cover (deforestation) as simulated by the HYDE model (V + H), and (iii) potential vegetation with anthropogenic land cover as simulated by the KK model (V + K). The KK model estimates are closer to a set of pollen-based reconstructions of vegetation cover than the HYDE model estimates. The climate-model results show that the simulated effects of deforestation depend on both local/regional climate and vegetation characteristics. At ~ 6 kBP the extent of simulated deforestation in Europe is generally small, but there are areas where deforestation is large enough to produce significant differences in summer temperatures of 0.5 – 1 °C. At ~ 0.2 kBP, simulated deforestation is much more extensive than previously assumed, in particular according to the KK model. This leads to significant temperature differences in large parts of Europe in both winter and summer. In winter, deforestation leads to lower temperatures because of the differences in albedo between forested and unforested areas, particularly in the snow-covered regions. In summer, deforestation leads to higher temperatures in central and eastern Europe since evapotranspiration from unforested areas is lower than from forests. Summer evaporation is already limited in the southernmost parts of Europe under potential vegetation conditions and, therefore, cannot become much lower. Accordingly, the albedo effect dominates also in summer, which implies that deforestation causes a decrease in temperatures. Differences in summer temperature due to deforestation range from -1 °C in south-western Europe to $+1$ °C in eastern Europe. The choice of anthropogenic land cover estimate has a significant influence on the simulated climate, but uncertainties in palaeoclimate

Regional climate model simulations for Europe at 6 k and 0.2 kyr BP

G. Strandberg et al.

Title Page

Abstract

Introduction

Conclusions

References

Tables

Figures



Back

Close

Full Screen / Esc

Printer-friendly Version

Interactive Discussion



proxy data for the two time periods do not allow for a thorough comparison with climate model results.

1 Introduction

Long before we started to emit CO₂ from fossil fuel combustion, humans already potentially had an influence on the climate system through deforestation and early agriculture (Ruddiman, 2005). Deforestation affects the climate at many scales, from microclimate to global climate (e.g. Bala et al., 2007). The effect on the global climate is conveyed by the increased amounts of CO₂ in the atmosphere from deforestation, and by the regional and local changes of land-surface properties (e.g. Forster et al., 2007). Such changes have a direct effect on the regional climate, including changes in albedo and energy fluxes between the land surface and the atmosphere (e.g. Pielke et al., 2011). Since forests generally have a lower reflectivity than unforested areas, the albedo effect from deforestation would lead to lower regional temperature. Reduced vegetation cover also means reduced evapotranspiration that leads to higher air temperature, but the amplitude of the evapotranspiration changes depend on local conditions, such as soil moisture availability (Ban-Weiss et al., 2011; de Noblet-Ducoudré, 2012). The effects from increased atmospheric CO₂ resulting from changing vegetation and land-use over the last 8000 yr have been previously discussed (e.g. Ruddiman, 2005; Pongratz et al., 2009a). The direct effects of past vegetation change have mostly been studied on a global scale (e.g. Brovkin et al., 2006; Pitman et al., 2009; Pongratz et al., 2009b, 2010; de Noblet-Ducoudré, 2012; Christidis et al., 2013).

Global climate models (GCM) are run on coarse spatial resolutions; therefore they can only reproduce large scale climate features. Regional climate models (RCM) preserve the large-scale climate features, but the higher spatial resolution in RCMs provides a better representation of the land-sea distribution and topography, which in turn allows a more detailed description of the regional climate (Rummukainen, 2010). This also applies to vegetation modelling. Only a detailed description of vegetation can ac-

CPD

9, 5785–5836, 2013

Regional climate model simulations for Europe at 6 k and 0.2 k yr BP

G. Strandberg et al.

Title Page

Abstract

Introduction

Conclusions

References

Tables

Figures

⏪

⏩

◀

▶

Back

Close

Full Screen / Esc

Printer-friendly Version

Interactive Discussion



Regional climate model simulations for Europe at 6 k and 0.2 kyr BP

G. Strandberg et al.

[Title Page](#)

[Abstract](#)

[Introduction](#)

[Conclusions](#)

[References](#)

[Tables](#)

[Figures](#)

[⏪](#)

[⏩](#)

[◀](#)

[▶](#)

[Back](#)

[Close](#)

[Full Screen / Esc](#)

[Printer-friendly Version](#)

[Interactive Discussion](#)

count for biogeophysical effects on climate at the regional scale (Wramneby et al., 2010). When evaluating model results by comparison with observations and/or proxies that represent local to regional environment conditions, and since we expect vegetation change to affect climate at the local/regional spatial scale, a high spatial resolution in the climate model is critical. To date there are no previous RCM-based studies of the

The present study investigates the direct effect from human-induced vegetation changes in Europe at the regional spatial scale. We do not study the indirect effects from changing atmospheric CO₂ concentration. This study is part of the LANDCLIM (LAND cover – CLIMate interactions in NW Europe during the Holocene) project that aims to quantify human-induced changes in regional vegetation/land cover in north-western Europe during the Holocene to assess the possible effects on the climate of two historical processes (compared with a baseline of present-day land cover): (i) climate-driven changes in vegetation and (ii) human-induced changes in land cover (Gaillard et al., 2010). Specifically this study asks (i) Does historical land-use influence the regional climate? (ii) How much does the RCM-simulated climate differ depending on the scenario of past anthropogenic land cover used? (iii) Which processes are important for climate-vegetation interaction? and (iv) to what extent are palaeoclimate proxy data effective at evaluating RCM-based simulation results?

We focus on two contrasting time periods in terms of climate and anthropogenic land cover change: the Mid-Holocene warm period (~ 6 kyrBP) and the Little Ice Age (~ 0.2 kyrBP). The Mid-Holocene was characterised by a relatively warm climate and low human impact on vegetation/land cover, while the Little Ice Age was cool and anthropogenic land-use was extensive. The 6 k time-window has the advantage of being widely used in model-data comparison studies of global climate models (e.g. Harrison et al., 1998; Masson et al., 1999; Kohfeld and Harrison, 2000; see the Palaeo-climate Modelling Intercomparison Project – PMIP – activities: pmip.lsce.ipsl.fr), which allows us to set our results in a wider perspective. We use a dynamic vegetation model, LPJ-GUESS (Smith et al., 2001), to simulate past climate-driven potential natural vegetation

and CH₄ are explicitly described. GHGs and solar irradiance changes from year to year and are read annually by the models. Table 1 summarizes the forcing from GHGs and insolation averaged over the two periods.

For snow in unforested areas, RCA3 has a prognostic albedo that varies between 0.6–0.85; the albedo decreases as snow ages. For snow-covered land areas in forest regions the albedo is set constant to 0.2. The snow-free albedo is set to 0.28 and 0.15 for unforested and forested areas, respectively. Leaf Area Index (LAI) is calculated as a function of the soil temperature with a lower limit set to 0.4, and upper limits to 2.3 (unforested) and 4.0 (deciduous forest). If deep soil moisture reaches the wilting point the LAI is set to its lower limit. LAI in coniferous forests is set constant to 4.0 regardless of soil moisture (Samuelsson et al., 2011).

RCA3 is run on a horizontal grid spacing of 0.44° (corresponding to approximately 50 km) over Europe with 24 vertical levels and a time step of 30 min. Data for initializing RCA3 are taken from ECHO-G. After that, every 12 h, RCA3 reads surface pressure, humidity, temperature and wind from ECHO-G along the lateral boundaries of the model domain, and sea surface temperature and sea-ice extent within the model domain. All RCA3 simulations have been run for 50 yr with 1 yr spin-up time, after which the effect of the initial conditions of atmosphere/land surface system are assumed to have faded (Giorgi and Mearns, 1999).

For each simulation of a 50 yr period we calculate the average of the nominal seasons winter (December, January and February; henceforth DJF) and summer (June, July and August; henceforth JJA). In addition, the diurnal cycle is analysed for some regions.

The statistical significance for the difference between the simulations is determined by a bootstrapping technique (Efron, 1979). 500 bootstrap samples are used to estimate the inter-annual variability of seasonal and annual means of temperature, precipitation, latent heat flux and albedo for each simulation. The difference between two simulations is compared with the estimated distribution of a parameter (e.g. temper-

CPD

9, 5785–5836, 2013

**Regional climate
model simulations for
Europe at 6 k and
0.2 kyr BP**

G. Strandberg et al.

Title Page

Abstract

Introduction

Conclusions

References

Tables

Figures

⏪

⏩

◀

▶

Back

Close

Full Screen / Esc

Printer-friendly Version

Interactive Discussion

ature) to see if the difference is statistically significant. We choose the 95 % level for significance.

2.1.3 The dynamic vegetation model LPJ-GUESS

LPJ-GUESS (Smith et al., 2001; Hickler et al., 2004, 2012) is used to simulate potential natural vegetation patterns consistent with the simulated climate in Europe during the two selected time windows. The model has been previously used to simulate past vegetation (Miller et al., 2008; Garreta et al., 2010; Kjellström et al., 2010; Strandberg et al., 2011) and to assess the effects of land-use on the global carbon cycle (Olofsson and Hickler 2008; Olofsson, 2013).

LPJ-GUESS is a process-based dynamic ecosystem model designed for application at regional to global spatial scales. It incorporates representations of terrestrial vegetation dynamics based on interactions between individual trees and shrubs and a herbaceous understory at neighbourhood (patch) scale (Hickler et al., 2004). It accounts for the effect of stochastically recurring disturbances for heterogeneity among patches in terms of accrued biomass, vegetation composition and structure at the landscape scale. The simulated vegetation is represented by Plant Functional Types (PFTs; Table 2) discriminated in terms of bioclimatic limits to survival and reproduction, leaf phenology, allometry, life-history strategy and aspects of physiology governing carbon balance and canopy gas-exchange. Differences between PFTs in combination with the present structure of the vegetation in each patch govern the partitioning of light and soil water among individuals as well as regeneration and mortality, affecting competition among PFTs and age/size classes of plants.

Inputs to the model are: temperature ($^{\circ}\text{C}$), precipitation (mm), net downward short-wave radiation at surface (Wm^{-2}) and wet day frequency (days) all in monthly time-steps provided by RCA3 at a 0.44° spatial resolution over Europe and annual atmospheric CO_2 concentration for the 6 k and 0.2 k time windows. The static, present-day soil texture data described in Sitch et al. (2003) were used during all simulations. The

**Regional climate
model simulations for
Europe at 6 k and
0.2 kyr BP**

G. Strandberg et al.

Title Page

Abstract

Introduction

Conclusions

References

Tables

Figures

⏪

⏩

◀

▶

Back

Close

Full Screen / Esc

Printer-friendly Version

Interactive Discussion

PFT determination was based on the European dominant species version described by Hickler et al. (2012) (Table 2).

2.1.4 The anthropogenic land cover models KK and HYDE

The historical ALCC scenarios most often used in climate modelling are HYDE (Klein Goldewijk et al., 2011), KK (Kaplan et al., 2009) and the scenarios of Pongratz et al. (2009). We have chosen HYDE and KK for this study because they represent the two extremes of the estimated ALCC for the two selected time windows. These ALCC models use similar estimates of past human population density, but differ in their estimates of land requirement per capita and the assessment of the effect of contrasting technological development between regions. Therefore, they provide significantly different scenarios of the extent of deforestation and land-use intensity (Gaillard et al., 2010; Boyle et al., 2011; Kaplan et al., 2011).

The KK (hereafter referred to as K) dataset represents the total amount of the land fraction used for agrarian activities at a 5' spatial resolution. The HYDE (hereafter referred to as H) land-use dataset includes information on the fraction of cropland, grassland and urban areas, also at a 5' spatial resolution. It was downloaded from the online database (<http://themasites.pbl.nl/en/themasites/hyde/download/index.html>) on 13 December 2011. The different land-use categories are summed up to represent the total fraction of anthropogenic deforestation. The upscaled (to a 0.5° resolution) versions of both datasets are used for the two selected time windows.

2.2 Alternative land cover descriptions used in the RCA3 runs

Potential natural land cover (hereafter referred to as V) for 6k and 0.2k is simulated using LPJ-GUESS (forced with results from RCA3). The resulting LAI per PFT and per grid cell is averaged over the modeling period for both time windows and then converted to foliage projective cover (FPC). The FPC is defined, applying the Lambert–Beer law

CPD

9, 5785–5836, 2013

Regional climate model simulations for Europe at 6 k and 0.2 kyr BP

G. Strandberg et al.

Title Page

Abstract

Introduction

Conclusions

References

Tables

Figures

⏪

⏩

◀

▶

Back

Close

Full Screen / Esc

Printer-friendly Version

Interactive Discussion



(Monsi and Saeki, 1953), as the area of ground covered by foliage directly above it (Sitch et al., 2003):

$$\text{FPC(PFT)} = 1.0 - \exp(-k \cdot (\text{LAI(PFT)}))$$

where k is the extinction coefficient (0.5).

The calculated species-specific FPC-values were summed up to three RCA3-specific PFTs (Table 2) per grid cell. The fraction of non-vegetated land is calculated by subtracting the sum of all the PFT-values per grid cell from one.

In order to obtain a description of the land cover including information on both natural and human-induced vegetation the LPJ-GUESS simulation results (V) are combined with the two ALCC simulations, K and H . The $V + K$ and $V + H$ vegetation descriptions are constructed by subtracting the ALCC fraction determined by K or H from one, and thereafter rescaling the PFT values provided by V to fit into the remaining space. The total unforested fraction is then calculated by summing up the ALCC K or H with the LPJ-GUESS simulated PFT Grass fractions in each grid cell.

To assess which land cover description might be the most reasonable to use, we compare the V , $V + H$ and $V + K$ descriptions with the pollen-based REVEALS estimates of vegetation cover produced by the LANDCLIM project (Gaillard et al., 2010; Mazier et al., 2012; Trondman et al., 2013). The LANDCLIM REVEALS vegetation database includes grid-cell based mean REVEALS estimates at a 1° resolution for 25 plant taxa, also grouped into 10 plant functional types (PFTs) and three land cover units (hereafter referred to as RCA3 PFTs). In this study we use the available REVEALS estimates of the three RCA3 PFTs at 6 k (203 grid cells) and 0.2 k (185 grid cells) (Table 2) to calculate the reconstructed fractions of forested (sum of coniferous and broad-leaved tree canopy) and unforested land cover. The simulated V , $V + H$ and $V + K$ land cover descriptions are recalculated to 100 % vegetation omitting the non-vegetated fraction and upscaled to a 1° spatial resolution. The agreement of the three sets of results is assessed by comparison of the dominant (> 50 %) land cover type (unforested or forested) between the sets.

**Regional climate
model simulations for
Europe at 6 k and
0.2 kyr BP**

G. Strandberg et al.

Title Page

Abstract

Introduction

Conclusions

References

Tables

Figures

⏪

⏩

◀

▶

Back

Close

Full Screen / Esc

Printer-friendly Version

Interactive Discussion



2.3 Proxy data of past climate

We use two proxy datasets of past climate for comparison with the RCA3 climate simulations at 6k and 0.2k: the LANDCLIM database of past climate proxy records, consisting mainly of site specific/point reconstructions of past climate based on non-pollen proxies; and the spatially explicit pollen-based climate reconstruction of Mauri et al. (2013). For the southern and eastern parts of the study area covered by the RCA3 simulations but not by the LANDCLIM database, we rely primarily on the non-pollen proxy-based climate reconstructions presented in Magny and Combourieu Nebout (2013), and in particular the synthesis of palaeohydrological changes and their climatic implications in the central Mediterranean region and its surroundings (Magny et al., 2013). The Mauri et al. (2013) reconstruction in the Mediterranean area is also compared to the pollen-based climate reconstructions in the Mediterranean region published by Peyron et al. (2013). The latter reconstructions are based on the multi-method approach that uses a combination of pollen-based weighted averaging, weighted-average partial least-squares regression, modern analogue technique (MAT), and non-metric multidimensional scaling/generalized additive model methods.

The LANDCLIM database includes palaeoecological and historical (written archives and instrumental measurements) datasets from 245 sites in western Europe north of the Alps for the two time windows 6k (5700–6200 BP) and 0.2k (1700–1800 AD) as well as for the time after 1960 AD. Climate reconstructions based on proxies of vegetation (plant macrofossils and pollen) are excluded from the database to avoid circular reasoning. The selected reconstructions are dated with multiple radiocarbon dates of terrestrial plant material, varve counts, tree rings, TIMS (thermal ionisation mass spectrometry) dated speleothems or historical records. In terms of absolute values of climate characteristics, these palaeoecological proxies provide reconstructions of primarily summer temperature (T) from e.g. diatom and chironomid records (July T) and tree ring index (July–August or June–September T). There are only very few quantitative reconstructions of precipitation and winter temperature, but a large number

**Regional climate
model simulations for
Europe at 6 k and
0.2 kyr BP**G. Strandberg et al.

[Title Page](#)[Abstract](#)[Introduction](#)[Conclusions](#)[References](#)[Tables](#)[Figures](#)[⏪](#)[⏩](#)[◀](#)[▶](#)[Back](#)[Close](#)[Full Screen / Esc](#)[Printer-friendly Version](#)[Interactive Discussion](#)

of relative records of cold/wet vs. warm/dry, winter precipitation (varve thickness in lake sediments) and relative changes in precipitation minus evaporation ($P - E$) from records such as peat humification, testate amoebae, cladocera, ^{13}C and ^{18}O of bulk carbonates or gastropod calcite and reconstructions of lake-level changes and glacier advances/retreats. To compare our model-simulated climate results, we used primarily proxies based on diatoms, tree rings and chironomids for summer temperatures, and proxies based on lake-level changes, varve thickness in lake sediments, and ^{13}C and ^{18}O in carbonates for relative changes in yearly $P - E$.

The climate reconstruction of Mauri et al. (2013) largely follows the Modern Analogue Technique (MAT) approach described in Davis et al. (2003), but it is based on much improved pollen datasets. The modern surface sample dataset was compiled from the European Modern Pollen Database (Davis et al., 2013) and represents a substantial improvement compared to that used in Davis et al. (2003), with an increase in the number of samples by $\sim 80\%$ (total 4287 sites). The fossil dataset includes 48% more sites (total 756 sites) compared with Davis et al. (2003), with this improvement in data coverage spread throughout Europe. The MAT approach calculates a pollen-climate transfer function to reconstruct palaeoclimate from fossil pollen data, where the fossil and modern pollen samples are matched using pollen assemblages grouped into PFTs (Table 2). The use of PFT groups allows a wider range of taxa to be included in the analysis without over-tuning the transfer function, and allows taxa to be included that may not be present in the modern pollen calibration dataset. Since PFT groups are largely defined according to their climatic affinities (Prentice et al., 1996), the approach also reduces the sensitivity of the transfer-function to non-climatic influences, such as human impact on vegetation, disease, ecological competition or succession, or soil processes. Approximate standard errors for the reconstruction were calculated following Bartlein et al. (2010) by assimilating samples at the interpolated spatial grid resolution, together with the standard error from the interpolation itself.

3 Results

3.1 LPJ-GUESS simulated vegetation

The simulated potential vegetation (V) at 6 k is characterised by a forest cover of > 90 % in most of Europe (Fig. 2). The areas with less than 50 % of forest cover (central Alps, Scandinavian mountains, northern Scandinavia and Iceland) are typically related to high elevations and/or latitudes. The simulated forest composition of northern and eastern Europe and elevated areas of central Europe is dominated by coniferous trees, while western and lowland Europe is dominated by broadleaved trees. The average HYDE anthropogenic land cover/deforestation (H) at 6 k is generally < 1 %; values > 5 % are restricted to some areas of southern Europe (Fig. 2). Therefore, the V + H land cover description does not differ markedly from V. The KK estimates of deforestation (K) are higher (> 4 % in average) and reach values > 50 % in southern Europe and restricted areas of southern Scandinavia, Belgium and the northern Alps. However, the additional unforested land predicted by HYDE and KK is negligible in comparison to the potential unforested land simulated by LPJ-GUESS, which explains why the V, V + H and V + K land cover descriptions do not differ significantly from each other at 6 k.

The V land cover description at 0.2 k shows little difference compared to V at 6 k (Fig. 2). The largest differences are found in Scandinavia where areas with less than 50 % of forest cover are much larger than they are at 6 k. The average H estimates of deforestation are ca. 10 %, but reach values > 50 % in southern Europe. The K estimates of anthropogenic unforested areas are > 40 % on average and the highest values (> 95 %) are found in southern Europe. Owing to the high K estimates in most western, central and southern Europe, the forest cover is considerably reduced in V + K in comparison to V + H and particularly to V.

3.2 Simulated climate

The overall features of the simulated 6 k_V and 0.2 k_V regional climate are comparable. Winter (DJF) mean temperatures range from -15°C in northern Europe to 10°C over the Iberian Peninsula (Figs. 3 and 4, upper left panels). In summer (JJA), the highest temperatures (ca. 20°C) occur in the Mediterranean region, while summer mean temperatures do not reach more than ca. 10°C in northern Scandinavia (Figs. 3 and 4, lower left panel). Summer temperatures at 6 k are ca. $0\text{--}2^{\circ}\text{C}$ warmer than at 0.2 k in most of Europe (Fig. 5). In winter, northern Europe is $1\text{--}2^{\circ}\text{C}$ warmer at 6 k than at 0.2 k, while large parts of central Europe are ca. 0.5°C colder.

The largest precipitation amounts in winter ($100\text{--}150\text{ mm month}^{-1}$) fall in the western parts and mountain ranges of the study area, while the smallest amounts ($30\text{--}60\text{ mm month}^{-1}$) are found in the eastern regions (Figs. 6 and 7, top rows). In summer, most precipitation ($60\text{--}100\text{ mm month}^{-1}$) falls over the land areas of the northern half of Europe, and the least around the Mediterranean ($0\text{--}50\text{ mm month}^{-1}$) (Figs. 6 and 7, bottom rows). The only significant differences in precipitation are seen in summer in parts of eastern and central Europe where 6 k_V is drier than 0.2 k_V by $10\text{--}20\text{ mm month}^{-1}$ (Fig. 8).

The difference between the simulated V climate and the V + H or V + K climate at 6 k is generally not statistically significant, but the V + K climate exhibits a few hotspots (southern Scandinavia, Belgium, north of the Alps) with summer temperatures $0.5\text{--}1^{\circ}\text{C}$ warmer than the V simulation (Fig. 3). Winter precipitation hardly differs between the 6 k V, V + H and V + K simulations, whereas small but statistically significant differences in summer precipitation (not more than -10 mm month^{-1}) between the 6 k V + K simulation and the other two 6 k simulations are found mostly in central Europe (Fig. 6). The unchanged precipitation pattern during winter in between the different RCA3 simulations might be due to the large influence of the large-scale atmospheric circulation during winter, inheriting the information from ECHO-G into RCA3. During summer this

Title Page

Abstract

Introduction

Conclusions

References

Tables

Figures

⏪

⏩

◀

▶

Back

Close

Full Screen / Esc

Printer-friendly Version

Interactive Discussion

effect is much lesser and more regional-to-local scale effects influence precipitation patterns.

At 0.2 k, deforestation (V + H and V + K) leads to lower winter (DJF) temperatures than potential vegetation (V) (Fig. 4, top row). The lower temperatures are confined to the Alps and parts of eastern Europe in the V + H simulation, while they are found in all of eastern Europe and southern Scandinavia in the V + K simulation, in some regions with as much as a 1–1.5 °C difference between the V + K and V simulations. However, the winter temperature differences between all simulations are statistically significant only in parts of eastern Europe. Summer (JJA) temperatures at 0.2 k are also lower (Fig. 4, bottom row), but only in the Mediterranean region, again most pronounced in the V + K simulation. Conversely, higher summer temperatures by up to 1 °C in parts of eastern Europe are a particular feature in the V + K simulation at 0.2 k. Summer precipitation is lower by 0–20 mm month⁻¹ in scattered parts of central and southern Europe in the V + H simulation at 0.2 k, while it is lower in all regions where the simulated forest fraction is reduced by more than 50 % in the V + K simulation, with statistically significant differences of –10 to –30 mm month⁻¹ in most of Europe (Fig. 7). Differences in winter precipitation between the simulations are very small.

The difference between the 6 k and 0.2 k simulations (6–0.2 k) greatly depends on the vegetation description used in the climate-model runs, i.e. V, V + H or V + K (Figs. 5 and 8). The climate simulations using vegetation descriptions with high values of deforestation (V + K) yield larger 6–0.2 k differences in summer temperature in south-west Europe (by 1–2 °C higher) than in eastern Europe (by ca. 1 °C). High values of deforestation at 0.2 k yield larger differences in (i) winter temperatures in eastern Europe (by 1–2 °C higher at 0.2 k than at 6 k), while small or no differences are seen in the rest of Europe (Fig. 5), and (ii) summer precipitation in south-east Europe (by around 30 mm month⁻¹ higher at 0.2 k than 6 k). In contrast, large deforestation at 0.2 k leads to smaller differences in winter precipitation between 0.2 k and 6 k in central Europe (Fig. 8).

Regional climate model simulations for Europe at 6 k and 0.2 kyr BP

G. Strandberg et al.

[Title Page](#)[Abstract](#)[Introduction](#)[Conclusions](#)[References](#)[Tables](#)[Figures](#)[⏪](#)[⏩](#)[◀](#)[▶](#)[Back](#)[Close](#)[Full Screen / Esc](#)[Printer-friendly Version](#)[Interactive Discussion](#)

The general effect of changes in the extent of deforestation on the simulated climate is a change in the amplitude in temperature and/or precipitation differences between 6 k and 0.2 k rather than a change in the geographical pattern of those differences.

3.3 Climate response to land-use changes

5 The largest differences in seasonal mean temperature and precipitation between the RCA3 simulations are found at 0.2 k between the V and V + K simulations. In order to assess the processes behind land cover-climate interactions, we analyse the annual cycle of temperature and latent heat flux at 0.2 k for three regions with particularly large deforestation, but different climate responses (see section above): Western Europe (WE), Eastern Europe (EE) and the Iberian Peninsula (IB). For each region, 3 × 3 grid
10 boxes are selected (Fig. 1).

In winter, lower temperatures due to deforestation are best explained by the albedo effect. The albedo is highest in the V + K simulation since low herb vegetation has a higher albedo than forests (Fig. 9, left column). The difference in albedo is even
15 higher during the snow season, since unforested areas are more readily covered by snow. Moreover, the effect increases in late winter/spring because of more incoming sunlight. Hence, deforestation leads to larger differences in winter temperature in the North/East, where the snow season is longer, than in the West/South.

When vegetation starts to be active in spring, the albedo effect is counteracted by
20 differences in latent heat flux. Generally, the larger biomass of forests compared to low vegetation leads to more evapotranspiration and, consequently, lower temperatures in forested than in deforested regions (Fig. 9, centre and right columns). The differences between the two simulations in latent heat flux start earlier in the year in WE compared to EE (Fig. 10, bottom row). Moreover, latent heat flux is weaker in summer and the
25 difference between the V + K and V simulations is smaller in WE than in EE, which explains the relatively moderate temperature difference between the two simulations in summer for WE. WE is also much influenced by the large-scale weather systems from the Atlantic, which makes changes in the regional surface properties less important

Regional climate model simulations for Europe at 6 k and 0.2 kyr BP

G. Strandberg et al.

Title Page

Abstract

Introduction

Conclusions

References

Tables

Figures

⏪

⏩

◀

▶

Back

Close

Full Screen / Esc

Printer-friendly Version

Interactive Discussion



than in EE. The latent heat flux in IB is strongest already in spring. When soils are dry in summer, the latent heat flux is weak and, therefore, the difference between the V + K and V simulations is small. In that case, the change in albedo dominates over the change in latent heat flux, leading to lower summer temperatures.

Differences in precipitation also correlate with differences in latent heat flux (Figs. 7 and 9). Since differences in precipitation are caused primarily by a change in convective precipitation (not shown), it suggests that also convective precipitation changes as a result of deforestation. This would explain that 0.2 k is drier in EE than 6 k in the V + K simulations. Observations in the tropics have indeed shown that regional deforestation decreases precipitation (Spracklen et al., 2012).

4 Discussion

4.1 Comparison of the RCA3 simulated regional climate with palaeoclimate reconstructions

Studies of diatoms (Korhola et al., 2000; Rosén et al., 2001; Bigler et al., 2006), tree rings (Grudd, 2002; Helama et al., 2002) and chironomids (Rosén et al., 2001; Bigler et al., 2003; Hammarlund et al., 2004; Laroque and Hall, 2004; Velle et al., 2005) indicate a 6–0.2 k difference in summer temperature of 0.5–2 °C in Scandinavia which agrees with our simulations. Evidence from the presence of Mediterranean ostracods in the coastal waters of Denmark suggests that winter temperature at 6 k were up to 4–5 °C above present (Vork and Thomsen, 1996). Proxy records of relative precipitation indicate a drier climate at 6 k than at 0.2 k in Scandinavia (Digerfelt, 1988; Ikonen, 1993; Snowball and Sandgren, 1996; Hammarlund et al., 2003; Borgmark, 2005; Olsen, 2010), northern Germany (Niggeman et al., 2003) and the UK (Hughes et al., 2000), while there is no detectable difference in the Alps (Magny, 2004). Our simulations show similar general features (Figs. 5 and 8). Unfortunately, quantitative proxy based temperature estimates are mainly available for Scandinavia where differences

Regional climate model simulations for Europe at 6 k and 0.2 kyr BP

G. Strandberg et al.

Title Page

Abstract

Introduction

Conclusions

References

Tables

Figures

⏪

⏩

◀

▶

Back

Close

Full Screen / Esc

Printer-friendly Version

Interactive Discussion



between the simulated climates with alternative land use scenarios are small. Therefore, none of the simulated climates agrees significantly better with the proxies than the others.

In the Mediterranean region, independent non-pollen proxy-based data indicate contrasting patterns of palaeohydrological changes between the regions north and south of the ca. 40° N latitude (Magny et al., 2013). The proxies imply that 6 k (0.2 k) were dry (wet) north of 40° and wet (dry) south of 40°. The available data in the synthesis of Magny et al. (2013) also suggest that these contrasting palaeohydrological patterns operated throughout the Holocene, both on millennial and centennial scales. Moreover, the combination of lake-level records and fire data was shown to provide information on the summer moisture availability. Fire frequency depends on the duration and intensity of the dry season (Pausas, 2004; Vanni re et al., 2011), while the main proxies used in lake-level reconstructions are often related to precipitation during the warm season (dry in summer; Magny, 2007). The fire records published by Vanni re et al. (2011) indicate the same contrasting pattern between the north- and the south-western Mediterranean for the mid-Holocene (including 6 k), with dry summers in the north and humid summers in the south. The evidence presented in Magny et al. (2013) suggest that, in response to centennial-scale cooling events, drier climatic conditions developed in the south-central Mediterranean, while wetter conditions prevailed in the north-central Mediterranean. In general, the centennial phases of higher lake-level conditions in west-central Europe were shown to coincide with cooling events in the North Atlantic area (Bond et al., 2001; e.g. Magny, 2004, 2007) and decreases in solar activity before 7 k, and with a possible combination of NAO-type circulation and solar forcing since ca. 7 k onwards.

The 6–0.2 k difference in the simulated climate is generally small for all simulations (V, V + H and V + K) compared to the 6–0.2 k differences in the pollen-based climate reconstructions (PB reconstructions). Moreover, the geographical/spatial patterns of these 6–0.2 k differences show discrepancies between simulations and reconstructions (Fig. 5). The difference in summer temperatures ranges from ca. +1 °C in Scandinavia

Regional climate model simulations for Europe at 6 k and 0.2 kyr BP

G. Strandberg et al.

Title Page

Abstract

Introduction

Conclusions

References

Tables

Figures

⏪

⏩

◀

▶

Back

Close

Full Screen / Esc

Printer-friendly Version

Interactive Discussion



to evaluate the RCA3 results for summer temperatures in eastern Europe and winter precipitation.

The two climate regions identified by Magny et al. (2013) are not seen in the PB reconstructions of Mauri et al. (2013) and the RCA3 simulations, except a weak pattern of contrasting summer temperatures on both side of latitude 40° N in the RCA3 simulations. However, it should be noted that 6 k is within the transition period (6.4–4.5 k) between the two climate regimes before and after 4.5 k described by Magny et al. (2013), which may explain that the patterns around 6 k are difficult to capture both by the climate model and the PB reconstructions. Further, there is no equivalent in the non-pollen proxy-based palaeoclimatic records to the PB reconstruction of Mauri et al. (2013) in terms of higher winter precipitations at 6 k than at 0.2 k in Eastern Europe North of 40° N.

The comparison between climate model simulations and pollen based palaeoclimate data indicate that discrepancies occur in the geographical patterns of the differences in climate between 6 k and 0.2 k. This is particularly clear for temperatures in southern Europe, where model and proxies exhibit opposite signs of the difference in temperature, and for winter precipitation, where reconstructions exhibit much larger differences than the RCA3 simulations (Figs. 5 and 8). A wetter summer in western-central Europe at 0.2 k than at 6 k is in better agreement with the non-pollen proxy records (e.g. in the Jura mountains, Magny et al., 2013) than a drier western-central Europe as indicated in the PB reconstruction.

As the differences between the three model simulations (V, V + H and V + K) are generally smaller than the differences between the model simulations and the pollen-based reconstructions of past climate, it is not possible to identify the vegetation description (V, V + H or V + K) that provide the most coherent simulated climate for Europe at 6 k and 0.2 k.

CPD

9, 5785–5836, 2013

Regional climate model simulations for Europe at 6 k and 0.2 kyr BP

G. Strandberg et al.

Title Page

Abstract

Introduction

Conclusions

References

Tables

Figures



Back

Close

Full Screen / Esc

Printer-friendly Version

Interactive Discussion



4.2 Model simulations in a wider perspective

In this study, we use boundary conditions provided by the GCM ECHO-G. ECHO-G is one of many GCMs and the use of boundary conditions from another GCM may give different RCA3 results. Moreover, a different realisation of the climate with ECHO-G would likely result in a different RCA3 output as the impact of internal variability is large (Deser et al., 2012). In order to assess to what degree our results might be biased by the choice of one single GCM realisation, we compare our results with an ensemble of PMIP models. This ensemble represents uncertainties related both to the choice of GCM and to internal variability as each GCM starts with its own initial conditions. Figure 11 shows temperature difference vs. precipitation difference (6–0.2 k) for 7 PMIP GCMs, ECHO-G and RCA3. The differences are calculated for two large regions that are resolved at the scale of the GCMs, northern Europe (5–50° E, 55–70° N) and southern Europe (10° W–50° E, 35–55° N) (blue boxes in Fig. 1). All model results share common features, but show some differences; the spread between models is largest in summer precipitation and winter temperature in northern Europe and smallest in winter precipitation in southern Europe.

RCA3 follows ECHO-G to some extent, with the exception of summer precipitation in northern Europe. The land-sea distribution in the RCA3 simulations differs between 6 k and 0.2 k (Fig. 1) with some grid boxes being sea at 6 k and land at 0.2 k. This difference leads to more convective precipitation at 0.2 k than at 6 k for these coastal regions (cf. Fig. 8). A similar effect is seen along the coast of the Mediterranean Sea. In ECHO-G the land-sea distribution is constant through time. Thus, for some coastal areas, the precipitation difference between 6 k and 0.2 k is negative in the RCA3 simulation and positive in the ECHO-G simulation.

The choice of another GCM would obviously provide different results, but the difference is difficult to quantify since there are no systematic differences between the models, and RCA3 partly produces its “own” climate. Interestingly enough, all of the GCMs show positive summer temperature differences between 6 k and 0.2 k. It indi-

CPD

9, 5785–5836, 2013

Regional climate model simulations for Europe at 6 k and 0.2 kyr BP

G. Strandberg et al.

Title Page

Abstract

Introduction

Conclusions

References

Tables

Figures

⏪

⏩

◀

▶

Back

Close

Full Screen / Esc

Printer-friendly Version

Interactive Discussion

Regional climate model simulations for Europe at 6 k and 0.2 kyr BP

G. Strandberg et al.

Title Page

Abstract

Introduction

Conclusions

References

Tables

Figures

⏪

⏩

◀

▶

Back

Close

Full Screen / Esc

Printer-friendly Version

Interactive Discussion

eas. On the other hand, pollen data from treeless, sparsely vegetated arctic-alpine environments often exhibit considerable amounts of boreal tree pollen (Lisytsyna et al., 2011; Hicks, 2001) that might lead to an over-estimation of tree cover in pollen-based reconstructions. Although the REVEALS model corrects in part for the combined effect of low pollen production and dispersal of local herbaceous vegetation and high pollen production and dispersal of boreal trees, the results may be biased by pollen transported on particularly large distances (> 200 km), such as pine and birch.

There is much less agreement between the simulated land cover and the REVEALS reconstruction at 0.2 k for the simulations V and V + H. The climate-driven vegetation (V) and least deforested land-cover (V + H) exhibit much less cover of unforested areas than the REVEALS reconstructions in central and western Europe. In contrast, the simulation V + K shows better agreement with the REVEALS reconstructions, which indicates that human-induced deforestation and the development of cultivated and grazed unforested areas greatly influenced vegetation cover in the study area at 0.2 k. These results agree with the comparison of Kaplan et al's KK scenarios with REVEALS estimates for five time windows of the Holocene from 6 k to present (Trondman et al., 2013). Therefore, the V + K vegetation simulation is regarded as the most reasonable land-cover description to be used in climate modelling experiments at 0.2 k.

However, the high REVEALS estimates of unforested areas at 0.2 k in large parts of the British Isles, Scotland in particular, are not found in any of the simulated vegetation descriptions. One possible explanation is the occurrence of vegetation types that are poorly simulated by the LPJ-GUESS model. The vegetation of the northern and western parts of the British Isles is today characterised by large acidic heath- and moorlands dominated by heather, grasses and mosses. Palaeoecological studies have shown that this type of vegetation developed from the Neolithic time (6 k and onwards) as a result from the interaction of anthropogenic land-use and climate change in the region (e.g. Tipping, 1994; Bennett, 1995; Bunting, 1996). The occurrence of heathland may also contribute to the higher REVEALS based openness than the LPJ-GUESS openness in parts of western Norway and Denmark.

The differences in the importance of the various biogeophysical processes depend on the land-cover descriptions used and local geographical characteristics.

5 Conclusions

This study demonstrates that past European anthropogenic land-cover changes prior to 1850 AD were large enough to influence the regional climate. The temperature response varied by $\pm 1^\circ\text{C}$ in summer depending on local/regional characteristics that can only be captured by high-resolution climate models such as RCA3.

The differences in simulated climate depend mainly on changes in the albedo and latent heat flux due to changes in vegetation cover. Which of the biogeophysical processes will be dominant depends on local/regional climate and vegetation characteristics. The results show that the effect of albedo dominates in winter, but that also latent heat flux plays an important role for the differences in simulated climate in summer. Therefore, a comprehensive model including these effects is required to study effects of changing land cover on climate. At 6 k the differences between the land-cover descriptions (V, V + H or V + K) are small, leading to little difference between the simulated climates. At 0.2 k the differences between the land-cover descriptions are large enough to result in significantly different simulated climates. Depending on the estimate of deforestation, the difference between simulations varies in some regions between -1 and 0°C in seasonal mean winter temperature, -1 and 1°C in summer temperature and -30 and 0 mm month^{-1} in summer precipitation.

Even though the difference in climate is significant between simulations using different land cover descriptions (V, V + H or V + K), it is not possible to assess which land-cover description is the most reasonable on the basis of a comparison with climate reconstructions inferred from palaeo proxies. This is because the uncertainties of the palaeoclimate reconstructions and the differences between them are at least as large as the differences between the climate simulations at both 6 k and 0.2 k. Nevertheless, it is clear that vegetation cover plays an important role for the regional climate and

Regional climate model simulations for Europe at 6 k and 0.2 kyr BP

G. Strandberg et al.

Title Page

Abstract

Introduction

Conclusions

References

Tables

Figures

⏪

⏩

◀

▶

Back

Close

Full Screen / Esc

Printer-friendly Version

Interactive Discussion



**Regional climate
model simulations for
Europe at 6 k and
0.2 kyr BP**

G. Strandberg et al.

[Title Page](#)[Abstract](#)[Introduction](#)[Conclusions](#)[References](#)[Tables](#)[Figures](#)[⏪](#)[⏩](#)[◀](#)[▶](#)[Back](#)[Close](#)[Full Screen / Esc](#)[Printer-friendly Version](#)[Interactive Discussion](#)

Bennett, K.: Post-glacial dynamics of pine (*Pinus sylvestris* L.) and pinewoods in Scotland, in: Our Pinewood Heritage, edited by: Aldhous, J. R., Proceedings of the Conference at Culloden Academy, Inverness, 23–39, 1995.

Berger, A. and Loutre, M. F.: Insolation values for the climate of the last 10 million years, *Quaternary Sci. Rev.*, 10, 29–317, 1991.

Bigler, C., Grahn, E., Larocque, I., Jeziorski, A., and Hall, R.: Holocene environmental change at Lake Njulla (999 m a.s.l.), northern Sweden: a comparison with four small nearby lakes along an altitudinal gradient, *J. Paleolimnol.*, 29, 13–29, 2003.

Bigler, C., Barnekow, L., Heinrichs, M. L., and Hall, R. I.: Holocene environmental history of Lake Vuolop Njakajaure (Abisko National Park, northern Sweden) reconstructed using biological proxy indicators, *Veg. Hist. Archaeobot.*, 15, 309–320, 2006.

Bond, G., Kromer, B., Beer, J., Muscheler, R., Evans, M. N., Showers, W., Hoffmann, S., Lotti-Bond, R., Hajdas, I., and Bonani, G.: Persistent solar influence on North Atlantic climate during the Holocene, *Science*, 294, 2130–2136, 2001.

Borgmark, A.: Holocene climate variability and periodicities in south-central Sweden interpreted from peat humification analysis, *Holocene*, 15, 387–395, 2005.

Boyle, J. F., Gaillard, M.-J., Kaplan, J. O., and Dearing, J. A.: Modelling prehistoric land use and carbon budgets: a critical review, *Holocene*, 21, 715–722, 2011.

Brovkin, V., Claussen, M., Driesschaert, E., Fichetef, T., Kicklighter, D., Loutre, M. F., Matthews, H. D., Ramankutty, N., Schaeffer, M., and Sokolov, A.: Biogeophysical effects of historical land cover changes simulated by six Earth system models of intermediate complexity, *Clim. Dynam.*, 26, 587–600, doi:10.1007/s00382-005-0092-6, 2006.

Bunting, M. J.: The development of heathland in Orkney, Scotland: pollen records from Loch of Knitchen (Rousay) and Loch of Torness (Hoy), *Holocene*, 6, 193–212, 1996.

Christidis, N., Stott, P. A., Hegerl, G. C., and Betts, R. A.: The role of land use change in the recent warming of daily extreme temperatures, *Geophys. Res. Lett.*, 40, 589–594, doi:10.1002/grl.50159, 2013.

Collins, P. M., Davis, B. A. S., and Kaplan, J. O.: The mid-Holocene vegetation of the Mediterranean region and southern Europe, and comparison with the present day, *J. Biogeogr.*, 39, 1848–1861, 2012.

Davis, B. A. S., Brewer, S., Stevenson, A. C., and Guiot, J.: The temperature of Europe during the Holocene reconstructed from pollen data, *Quaternary Sci. Rev.*, 22, 1701–1716, 2003.

Regional climate model simulations for Europe at 6 k and 0.2 kyr BP

G. Strandberg et al.

[Title Page](#)
[Abstract](#)
[Introduction](#)
[Conclusions](#)
[References](#)
[Tables](#)
[Figures](#)
[Back](#)
[Close](#)
[Full Screen / Esc](#)
[Printer-friendly Version](#)
[Interactive Discussion](#)

Davis, B. A. S., Zanon, M., Collins, P., Mauri, A., Bakker, J., Barboni, D., Barthelmes, A., Beaudouin, C., Bjune, A. E., Bozilova, E., Bradshaw, R. H. W., Brayshay, B. A., Brewer, S., Brugiapaglia, E., Bunting, J., Connor, S. E., Beaulieu, J.-L., Edwards, K., Ejarque, A., Fall, P., Florenzano, A., Fyfe, R., Galop, D., Giardini, M., Giesecke, T., Grant, M. J., Guiot, J., Jahns, S., Jankovská, V., Juggins, S., Kahrmann, M., Karpińska-Kołaczek, M., Kołaczek, P., Kühle, N., Kuneš, P., Lapteva, E. G., Leroy, S. A. G., Leydet, M., López Sáez, J. A., Masi, A., Matthias, I., Mazier, F., Meltsov, V., Mercuri, A. M., Miras, Y., Mitchell, F. J. G., Morris, J. L., Naughton, F., Nielsen, A. B., Novenko, E., Odgaard, B., Ortu, E., Overballe-Petersen, M. V., Pardoe, H. S., Peglar, S. M., Pidek, I. A., Sadori, L., Seppä, H., Severova, E., Shaw, H., Święta-Musznicka, J., Theuerkauf, M., Tonkov, S., Veski, S., Knaap, W. O., Leeuwen, J. F. N., Woodbridge, J., Zimny, M., and Kaplan, J. O.: The European Modern Pollen Database (EMPD) project, *Veg. Hist. Archaeobot.*, 22, 521–530, doi:10.1007/s00334-012-0388-5, 2013.

De Noblet-Ducoudré, N., Boisier, J.-P., Pitman, A., Bonan, G. B., Brovkin, V., Cruz, F., Delire, C., Gayler, V., van den Hurk, B. J. J. M., Lawrence, P. J., van der Molen, M. K., Müller, C., Reick, C. H., Strengers, B. J., and Voldoire, A.: Determining robust impacts of land-use-induced land cover changes on surface climate over North America and Eurasia: results from the first set of LUCID experiments, *J. Climate*, 25, 3261–3281, doi:10.1175/JCLI-D-11-00338.1, 2012

Deser, C., Knutti, R., Solomon, S., and Phillips, A. S.: Communication of the role of natural variability in future North American climate, *Nat. Clim. Change*, 2, 775–779, doi:10.1038/nclimate1562, 2012.

Digerfeldt, G.: Reconstruction and regional correlation of Holocene lake-level fluctuations in Lake Bysjön, South Sweden, *Boreas*, 17, 165–182, 1998.

Efron, B.: Bootstrap methods: another look at the jackknife, *Ann. Stat.*, 7, 1–26, 1979.

Flückiger, J., Monnin, E., Stauffer, B., Schwander, J., Stocker, T., Chappellaz, J., Raynaud, D., and Barnola, J. M.: High resolution Holocene N₂O ice core record and its relationship with CH₄ and CO₂, *Global Biogeochem. Cy.*, 16, 10-1–10-8, doi:10.1029/2001GB001417, 2002.

Forster, P., Ramaswamy, V., Artaxo, P., Berntsen, T., Betts, R., Fahey, D. W., Haywood, J., Lean, J., Lowe, D. C., Myhre, G., Nganga, J., Prinn, R., Raga, G., Schulz, M., and Van Dorland, R.: Radiative forcing of climate change, in: *Climate Change 2007: The Physical Science Basis, Contribution of Working Group I to the Fourth Assessment Report of the Intergovernmental Panel on Climate Change*, edited by: Solomon, S., Qin, D., Manning, M.,

Regional climate model simulations for Europe at 6 k and 0.2 kyr BP

G. Strandberg et al.

[Title Page](#)[Abstract](#)[Introduction](#)[Conclusions](#)[References](#)[Tables](#)[Figures](#)[⏪](#)[⏩](#)[◀](#)[▶](#)[Back](#)[Close](#)[Full Screen / Esc](#)[Printer-friendly Version](#)[Interactive Discussion](#)

- Chen, Z., Marquis, M., Averyt, K. B., Tignor, M., and Miller, H. L., Cambridge University Press, Cambridge and New York, NY, 129–234, 2007.
- Fyfe, R. M., Twiddle, C., Sugita, S., Gaillard, M.-J., Barratt, P., Caseldine, C. J., Dodson, J., Edwards, K. J., Farrell, M., Froyd, C., Grant, M. J., Huckerby, E., Innesm, J. B., Shawn, H., and Walle, M.: The Holocene vegetation cover of Britain and Ireland: overcoming problems of scale and discerning patterns of openness, *Quaternary Sci. Rev.*, 73, 132–148, 2013.
- Gaillard, M.-J.: Archaeological applications, in: *The Encyclopedia of Quaternary Science 3*, edited by: Elias, S. A., Elsevier, Amsterdam, 880–904, 2013.
- Gaillard, M.-J., Sugita, S., Mazier, F., Trondman, A.-K., Broström, A., Hickler, T., Kaplan, J. O., Kjellström, E., Kokfelt, U., Kuneš, P., Lemmen, C., Miller, P., Olofsson, J., Poska, A., Rundgren, M., Smith, B., Strandberg, G., Fyfe, R., Nielsen, A. B., Alenius, T., Balakauskas, L., Barnekow, L., Birks, H. J. B., Bjune, A., Björkman, L., Giesecke, T., Hjelle, K., Kalnina, L., Kangur, M., van der Knaap, W. O., Koff, T., Lagerås, P., Latałowa, M., Leydet, M., Lechterbeck, J., Lindbladh, M., Odgaard, B., Peglar, S., Segerström, U., von Stedingk, H., and Seppä, H.: Holocene land-cover reconstructions for studies on land cover-climate feedbacks, *Clim. Past*, 6, 483–499, doi:10.5194/cp-6-483-2010, 2010.
- Giorgi, F. and Mearns, L. O.: Introduction to special section: regional climate modelling revisited, *J. Geophys. Res.*,
- Gómez-Navarro, J. J., Montávez, J. P., Jerez, S., Jiménez-Guerrero, P., Lorente-Plazas, R., González-Rouco, J. F., and Zorita, E.: A regional climate simulation over the Iberian Peninsula for the last millennium, *Clim. Past*, 7, 451–472, doi:10.5194/cp-7-451-2011, 2011.
- Gómez-Navarro, J. J., Montávez, J. P., Jiménez-Guerrero, P., Jerez, S., Lorente-Plazas, R., González-Rouco, J. F., and Zorita, E.: Internal and external variability in regional simulations of the Iberian Peninsula climate over the last millennium, *Clim. Past*, 8, 25–36, doi:10.5194/cp-8-25-2012, 2012.
- Goosse, H., Guiot, J., Mann, M. E., Dubinkina, S., and Sallaz-Damaz, Y.: The medieval climate anomaly in Europe: comparison of the summer and annual mean signals in two reconstructions and in simulations with data assimilation, *Global Planet. Change*, 84–85, 35–47, 2012.
- Göttel, H., Alexander, J., Keup-Thiel, E., Rechid, D., Hagemann, S., Blome, T., Wolf, A., and Jacob, D.: Influence of changed vegetation fields on regional climate simulations in the Barents Sea Region, *Climatic Change*, 87, 35–50, doi:10.1007/s10584-007-9341-5, 2008.

Regional climate model simulations for Europe at 6 k and 0.2 kyr BP

G. Strandberg et al.

[Title Page](#)

[Abstract](#)

[Introduction](#)

[Conclusions](#)

[References](#)

[Tables](#)

[Figures](#)

[⏪](#)

[⏩](#)

[◀](#)

[▶](#)

[Back](#)

[Close](#)

[Full Screen / Esc](#)

[Printer-friendly Version](#)

[Interactive Discussion](#)

- Graham, L. P., Olsson, J., Kjellström, E., Rosberg, J., Hellström, S.-S., and Berndtsson, R.: Simulating river flow to the Baltic Sea from climate simulations over the past millennium, *Boreal Environ. Res.*, 14, 173–182, 2009.
- Grudd, H.: A 7400-year tree-ring chronology in northern Swedish Lapland: natural climatic variability expressed on annual to millennial timescales, *Holocene*, 12, 657–665, 2002.
- Hammarlund, D., Björck, S., Buchardt, B., Israelson, C., and Thomsen, C. T.: Rapid hydrological changes during the Holocene revealed by stable isotope records of lacustrine carbonates from Lake Igelsjön, southern Sweden, *Quaternary Sci. Rev.*, 22, 353–370, 2003.
- Hammarlund, D., Velle, G., Wolfe, B. B., Edwards, T. W. D., Barnekow, L., Bergman, J., Holmgren, S., Lamme, S., Snowball, I., Wohlfarth, B., and Possnert, G.: Palaeolimnological responses to Holocene forest retreat in the Scandes Mountains, west-central Sweden, *Holocene*, 14, 862–876, 2004.
- Harrison, S. P., Jolly, D., Laarif, F., Abe-Ouchi, A., Dong, B., Herterich, K., Hewitt, C., Jousaume, S., Kutzbach, J. E., Mitchell, J., de Noblet, N., and Valdes, P.: Intercomparison of simulated global vegetation distributions in response to 6 kyr BP orbital forcing, *J. Climate*, 11, 2721–2742, 1998.
- Helama, S., Lindholm, M., Timonen, M., Meriläinen, J., and Eronen, M.: The supra-long Scots pine tree-ring record for Finnish Lapland, Part 2: Interannual to centennial variability in summer temperatures for 7500 years, *Holocene*, 12, 681–687, 2002.
- Hellman, S., Gaillard, M.-J., Broström, A., and Sugita, S.: The REVEALS model, a new tool to estimate past regional plant abundance from pollen data in large lakes – validation in southern Sweden, *J. Quaternary Sci.*, 23, 21–42, 2008.
- Hickler, T., Vohland, K., Feehan, J., Miller, P. A., Smith, B., Costa, L., Giesecke, T., Fronzek, S., Carter, T. R., Cramer, W., Kühn, I., and Sykes, M. T.: Projecting the future distribution of European potential natural vegetation zones with a generalized, tree species-based dynamic vegetation model, *Global Ecol. Biogeogr.*, 21, 50–63, 2012.
- Hicks, S.: The use of annual arboreal pollen deposition values for delimiting tree-lines in the landscape and exploring models of pollen dispersal, *Rev. Palaeobot. Palynol.*, 117, 1–29, 2001.
- Hughes, P. D. M., Barber, K. E., Langdon, P. G., and Mauquoy, D.: Mire-development pathways and palaeoclimatic records from a full Holocene peat archive at Walton Moss, Cumbria, England, *Holocene*, 10, 465–479, 2000.

Regional climate model simulations for Europe at 6 k and 0.2 kyr BP

G. Strandberg et al.

[Title Page](#)[Abstract](#)[Introduction](#)[Conclusions](#)[References](#)[Tables](#)[Figures](#)[⏪](#)[⏩](#)[◀](#)[▶](#)[Back](#)[Close](#)[Full Screen / Esc](#)[Printer-friendly Version](#)[Interactive Discussion](#)

- Ikonen, L.: Holocene Development and Peat Growth of the Raised Bog Pesänsuo in South-western Finland, *Bulletin*, vol. 370, Geological Survey of Finland, Espoo, 1993.
- Jahn, A., Claussen, M., Ganopolski, A., and Brovkin, V.: Quantifying the effect of vegetation dynamics on the climate of the Last Glacial Maximum, *Clim. Past*, 1, 1–7, doi:10.5194/cp-1-1-2005, 2005.
- 5 Kaplan, J., Krumhardt, K., and Zimmermann, N.: The prehistoric and preindustrial deforestation of Europe, *Quaternary Sci. Rev.*, 28, 3016–3034, 2009.
- Kaspar, F., Spangehl, T., and Cubasch, U.: Northern hemisphere winter storm tracks of the Eemian interglacial and the last glacial inception, *Clim. Past*, 3, 181–192, doi:10.5194/cp-3-181-2007, 2007.
- 10 Kjellström, E., Brandefelt, J., Näslund, J. O., Smith, B., Strandberg, G., Voelker, A. H. L., and Wohlfarth, B.: Simulated climate conditions in Fennoscandia during a MIS 3 stadial, *Boreas*, 10, 436–456, doi:10.1111/j.1502-3885.2010.00143.x, 2010.
- Kjellström, E., Nikulin, G., Hansson, U., Strandberg, G., and Ullerstig, A.: 21st century changes in the European climate: uncertainties derived from an ensemble of regional climate model simulations, *Tellus A*, 63, 24–40, 2011.
- 15 Kleidon, A., Fraedrich, K., and Heimann, M.: A green planet versus a desert world: estimating the maximum effect of vegetation on the land surface climate, *Climatic Change*, 44, 471–493, 2000.
- 20 Klein Goldewijk, K., Beusen, A., and Janssen, P.: Long term dynamic modeling of global population and built-up area in a spatially explicit way, *HYDE 3.1, Holocene*, 20, 565–573, 2010.
- Kohfeld, K. E. and Harrison, S. P.: How well can we simulate past climates? Evaluating the models using global palaeoenvironmental datasets, *Quaternary Sci. Rev.*, 19, 321–346, 2000.
- Korhola, A., Weckström, J., Holmström, L., and Erästö, P.: A quantitative Holocene climatic record from diatoms in northern Fennoscandia, *Quaternary Res.*, 54, 284–294, 2000.
- 25 Laroque, I. and Hall, R. I.: Holocene temperature estimates and chironomid community composition in the Abisko valley, northern Sweden, *Quaternary Sci. Rev.*, 23, 2453–2465, 2004.
- Legutke, S. and Voss, R.: The Hamburg Atmosphere-Ocean Coupled Circulation Model ECHOG, DKRZ-Report, German Climate Computer Centre (DKRZ), Hamburg, Germany, 1999.
- 30 Lisytsyna, O. V., Giesecke, T., and Hicks, S.: Exploring pollen percentage threshold values as an indication for the regional presence of major European trees, *Rev. Palaeobot. Palynol.*, 166, 311–324, 2011.

Regional climate model simulations for Europe at 6 k and 0.2 kyr BP

G. Strandberg et al.

[Title Page](#)[Abstract](#)[Introduction](#)[Conclusions](#)[References](#)[Tables](#)[Figures](#)[⏪](#)[⏩](#)[◀](#)[▶](#)[Back](#)[Close](#)[Full Screen / Esc](#)[Printer-friendly Version](#)[Interactive Discussion](#)

Ljungqvist, F. C., Krusic, P. J., Brattström, G., and Sundqvist, H. S.: Northern Hemisphere temperature patterns in the last 12 centuries, *Clim. Past*, 8, 227–249, doi:10.5194/cp-8-227-2012, 2012.

Magny, M.: Holocene climate variability as reflected by mid-European lake-level fluctuations and its probable impact on prehistoric human settlements, *Quatern. Int.*, 113, 65–79, 2004.

Magny, M.: Holocene fluctuations of lake levels in west-central Europe: methods of reconstruction, regional pattern, palaeoclimatic significance and forcing factors, in: *Encyclopedia of Quaternary Science*, edited by: Elias, S., Elsevier, Oxford, 1389–1399, 2007.

Magny, M. and Combourieu Nebout, N.: Holocene changes in environment and climate in the central Mediterranean as reflected by lake and marine records, *Clim. Past*, 9, 1447–1454, doi:10.5194/cp-9-1447-2013, 2013.

Magny, M., Combourieu-Nebout, N., de Beaulieu, J. L., Bout-Roumazeilles, V., Colombaroli, D., Desprat, S., Francke, A., Joannin, S., Ortu, E., Peyron, O., Revel, M., Sadori, L., Siani, G., Sicre, M. A., Samartin, S., Simonneau, A., Tinner, W., Vannièrè, B., Wagner, B., Zanchetta, G., Anselmetti, F., Brugiapaglia, E., Chapron, E., Debret, M., Desmet, M., Didier, J., Essallami, L., Galop, D., Gilli, A., Haas, J. N., Kallel, N., Millet, L., Stock, A., Turon, J. L., and Wirth, S.: North–south palaeohydrological contrasts in the central Mediterranean during the Holocene: tentative synthesis and working hypotheses, *Clim. Past*, 9, 2043–2071, doi:10.5194/cp-9-2043-2013, 2013.

Masson, V., Cheddadi, R., Braconnot, P., Joussaume, S., Texier, D., and PMIP participants: Mid-Holocene climate in Europe: what can we infer from PMIP model-data comparisons?, *Clim. Dynam.*, 15, 163–182, 1999.

Mauri, A., Davis, B. A. S., Collins, P. M., and Kaplan, J. O.: The influence of atmospheric circulation on the mid-Holocene climate of Europe: a data-model comparison, *Clim. Past Discuss.*, 9, 5569–5592, doi:10.5194/cpd-9-5569-2013, 2013.

Mazier, F., Gaillard, M.-J., Kuneš, P., Sugita, S., Trondman, A.-K., and Broström, A.: Testing the effect of site selection and parameter setting on REVEALS-model estimates of plant abundance using the Czech Quaternary Palynological Database, *Rev. Palaeobot. Palynol.*, 187, 38–49, 2012.

Nielsen, A. B., Giesecke, T., Theuerkauf, M., Feeser, I., Behre, K.-E., Beug, H.-J., Chen, S.-H., Christiansen, J., Dörfler, W., Endtmann, E., Jahns, S., de Klerk, P., Köhl, N., Latałowa, M., Vad Odgaard, B., Rasmussen, P., Raal Stockholm, J., Voigt, R., Wiethold, J., and Wolters, S.:

**Regional climate
model simulations for
Europe at 6 k and
0.2 kyr BP**G. Strandberg et al.

[Title Page](#)[Abstract](#)[Introduction](#)[Conclusions](#)[References](#)[Tables](#)[Figures](#)[⏪](#)[⏩](#)[◀](#)[▶](#)[Back](#)[Close](#)[Full Screen / Esc](#)[Printer-friendly Version](#)[Interactive Discussion](#)

Quantitative reconstructions of changes in regional openness in north-central Europe reveal new insights into old questions, *Quaternary Sci. Rev.*, 47, 131–149, 2012.

Nielsen, A. B., Kokfelt, U., Rundgren, M., and Gaillard, M.-J.: A review of proxy based climate reconstructions for Northwest Europe in the time slices 6000 BP and 200 BP, in preparation, 2013.

Niggeman, S., Mangini, A., Richter, D. K., and Wurth., G.: A paleoclimate record of the last 17.600ears from the B7 cave, Sauerland, Germany, *Quaternary Sci. Rev.*, 22, 555–567, 2003.

Nikulin, G., Kjellström, E., Hansson, U., Strandberg, G., and Ullerstig, A.: Evaluation and future projections of temperature, precipitation and wind extremes over Europe in an ensemble of regional climate simulations, *Tellus A*, 63, 41–55, 2011.

Olsen, J., Noe-Nygaard, N., and Wolfe, B. B.: Mid to Late Holocene climate variability and anthropogenic impacts; multi-proxy evidence from lake Bliden, Denmark, *J. Paleolimnol.*, 43, 323–343, 2010.

Pausas, J. G.: Changes in fire and climate in the eastern Iberian Peninsula (Mediterranean basin), *Climatic Change*, 63, 337–350, 2004.

Peltier, W. R.: Global glacial isostasy and the surface of the ice-age circulation. Earth: the ICE-5G (VM2) model and GRACE, *Annu. Rev. Earth. Pl. Sc.*, 32, 111–149, 2004.

Peyron, O., Guiot, J., Cheddadi, R., Tarasov, P., Reille, M., de Beaulieu, J.-L., Bottema, S., and Andrieu, V.: Climatic reconstruction in Europe for 18,000 yr B.P. from pollen data, *Quaternary Res.*, 49, 183–196, 1998.

Peyron, O., Magny, M., Goring, S., Joannin, S., de Beaulieu, J.-L., Brugiapaglia, E., Sadori, L., Garfi, G., Kouli, K., Ioakim, C., and Combourieu-Nebout, N.: Contrasting patterns of climatic changes during the Holocene across the Italian Peninsula reconstructed from pollen data, *Clim. Past*, 9, 1233–1252, doi:10.5194/cp-9-1233-2013, 2013.

Pielke Sr., R. A., Pitman, A., Niyogi, D., Mahmood, R., McAlpine, C., Hossain, F., Klein Goldewijk, K., Nair, U., Betts, R., Fall, S., Reichstein, M., Kabat, P., and de Noblet, N.: Land use/land cover changes and climate: modeling analysis and observational evidence, *WIREs Clim. Change*, 2, 828–850, doi:10.1002/wcc.144, 2011.

Pitman, A. J., de Noblet-Ducoudre, N., Cruz, F. T., Davin, E. L., Bonan, G. B., Brovkin, V., Claussen, M., Delire, C., Ganzeveld, L., Gayler, V., van den Hurk, B. J. J. M., Lawrence, P. J., van der Molen, M. K., Muller, C., Reick, C. H., Seneviratne, S. I., Strengers, B. J., and Voldoire, A.: Uncertainties in climate responses to past land cover

**Regional climate
model simulations for
Europe at 6 k and
0.2 kyr BP**

G. Strandberg et al.

[Title Page](#)[Abstract](#)[Introduction](#)[Conclusions](#)[References](#)[Tables](#)[Figures](#)[⏪](#)[⏩](#)[◀](#)[▶](#)[Back](#)[Close](#)[Full Screen / Esc](#)[Printer-friendly Version](#)[Interactive Discussion](#)

- Schimanke, S., Meier, H. E. M., Kjellström, E., Strandberg, G., and Hordoir, R.: The climate in the Baltic Sea region during the last millennium simulated with a regional climate model, *Clim. Past*, 8, 1419–1433, doi:10.5194/cp-8-1419-2012, 2012.
- 5 Sitch, S., Smith, B., Prentice, I. C., Arneth, A., Bondeau, A., Cramer, W., Kaplan, J. O., Levis, S., Lucht, W., Sykes, M. T., Thonicke, K., and Venevsky, S.: Evaluation of ecosystem dynamics, plant geography and terrestrial carbon cycling in the LPJ dynamic global vegetation model, *Glob. Change Biol.*, 9, 161–185, 2003.
- Smith, B., Prentice, I. C., and Sykes, M. T.: Representation of vegetation dynamics in modelling of terrestrial ecosystems: comparing two contrasting approaches within European climate space, *Global Ecol. Biogeogr.*, 10, 621–637, 2001.
- 10 Snowball, I. and Sandgren, P.: Lake sediment studies of Holocene glacial activity, northern Sweden: contrasts in interpretation, *Holocene*, 6, 367–372, 1996.
- Solanki, S. K., Usoskin, I. G., Kromer, B., Schussler, M., and Beer, J.: Unusual activity of the Sun during recent decades compared to the previous 11,000 years. *Nature*, 431, 1084–1087, 2004.
- 15 Spracklen, D. V., Arnold, S. R., and Taylor, C. M.: Observations of increased tropical rainfall preceded by air passage over forests, *Nature*, 489, 282–286, doi:10.1038/nature11390, 2012.
- Strandberg, G., Brandefelt, J., Kjellström, E., and Smith, B.: High-resolution regional simulation of the last glacial maximum climate in Europe, *Tellus A*, 63, 107–125, 2011.
- 20 Sugita, S.: Theory of quantitative reconstruction of vegetation I: pollen from large sites REVEALS regional vegetation composition, *Holocene*, 17, 229–241, 2007.
- Tipping, R.: The form and fate of Scotland's woodlands, *Pwc Soc. Antiq. Scot.*, 124, 1–54, 1994.
- Trondman, A.-K., Gaillard, M.-J., Sugita, S., Mazier, F., Fyfe, R., Lechterbeck, J., Marquer, L., Nielsen, A. B., Twiddle, C., Barratt, P., Birks, H. J. B., Bjune, A. E., Caseldine, C., David, R., Dodson, J., Dörfler, W., Fischer, E., Giesecke, T., Hultberg, T., Kangur, M., Kuneš, P., Lat-alowa, M., Leydet, M., Lindbalhd, M., Mitchell, F., Odgaard, B., Peglar, S. M., Persson, T., Rösch, M., van der Knaap, P., van Geel, B., Smith, A., and Wick, L.: Pollen-based land-cover reconstructions for the study of past vegetation-climate interactions in NW Europe at 0.2 k, 0.5 k, 3 k and 6 k years before present, *J. Biogeogr.*, submitted, 2013.
- 30 Vannièrè, B., Colombaroli, D., Chapron, E., Leroux, A., Tinner, W., and Magny, M.: Climate versus human-driven fire regime in Mediterranean landscapes: the Holocene record of Lago dell'Accesa (Tuscany, Italy), *Quaternary Sci. Rev.*, 27, 1181–1196, 2008.

**Regional climate
model simulations for
Europe at 6 k and
0.2 kyr BP**G. Strandberg et al.

[Title Page](#)[Abstract](#)[Introduction](#)[Conclusions](#)[References](#)[Tables](#)[Figures](#)[⏪](#)[⏩](#)[◀](#)[▶](#)[Back](#)[Close](#)[Full Screen / Esc](#)[Printer-friendly Version](#)[Interactive Discussion](#)

- Velle, G., Brooks, S. J., Birks, H. J. B., and Willassen, E.: Chironomids as a tool for inferring Holocene climate: an assessment based on six sites in southern Scandinavia, *Quaternary Sci. Rev.*, 24, 1429–1462, 2005.
- 5 Vork, K. A. and Thomsen, E.: Lusitanian/Mediterranean ostracods in the Holocene of Denmark: implications for the interpretation of winter temperatures during the postglacial temperature maximum, *Holocene*, 6, 423–432, 1996.
- 10 Wagner, S., Widmann, M., Jones, J., Haberzettl, T., Lücke, A., Mayr, C., Ohlendorf, C., Schäbitz, F., and Zolitschka, B.: Transient simulations, empirical reconstructions and forcing mechanism for the Mid-holocene hydrological climate in Southern Patagonia, *Clim. Dynam.*, 29, 333–355, 2007.
- Wolf, A., Callaghan, T. V., and Larson, K.: Future changes in vegetation and ecosystem function of the Barents Region, *Climatic Change*, 87, 51–73, 2008.
- 15 Wramneby, A., Smith, B., and Samuelsson, P.: Hot spots of vegetation-climate feedbacks under future greenhouse forcing in Europe, *J. Geophys. Res.*, 115, D21119, doi:10.1029/2010JD014307, 2010.
- Zorita, E., Gonzalez-Rouco, J. F., von Storch, H., Montavez, J. P., and Valero, F.: Natural and anthropogenic modes of surface temperature variations in the last thousand years, *Geophys. Res. Lett.*, 32, L08707, doi:10.1029/2004GL021563, 2005.

Regional climate model simulations for Europe at 6 k and 0.2 kyr BP

G. Strandberg et al.

Table 1. Summary of forcing conditions in the RCA3 simulations, see text for details. The amount of greenhouse gases and irradiance varies from year to year, the table shows average values.

Name	Period	Vegetation	Land-use	CO ₂ (ppm)	CH ₄ (ppb)	N ₂ O (ppb)	Total solar irradiance (W m ⁻²)
6 k_V	6 kBP	Potential 6 k	None	265	572	260	1364
6 k_V + H			HYDE				
6 k_V + K			KK				
0.2 k_V	0.2 kBP	Potential 0.2 k	None	277	710	277	1363
0.2 k_V + H			HYDE				
0.2 k_V + K			KK				

[Title Page](#)

[Abstract](#)

[Introduction](#)

[Conclusions](#)

[References](#)

[Tables](#)

[Figures](#)

[I◀](#)

[▶I](#)

[◀](#)

[▶](#)

[Back](#)

[Close](#)

[Full Screen / Esc](#)

[Printer-friendly Version](#)

[Interactive Discussion](#)

Table 2. The three plant functional types (PFTs) for regional climate model RCA3, LPJ-GUESS PFTs according to Hickler et al. (2012) and Wolf et al. (2008), LANDCLIM REVEALS taxa (Mazier et al., 2012) and modern analogue technique (MAT) PFTs adapted from Peyron et al. (1998).

RCA3 LCU	LPJ-GUESS PFT	LANDCLIM REVEALS taxa*	MAT PFT
Coniferous tree canopy	<i>Picea_abies</i>	<i>Picea</i>	Boreal evergreen/ cool-temperate conifer
	<i>Abies_alba</i>	<i>Abies</i>	
	<i>Pinus_sylvestris</i> , <i>P. halepensis</i>	<i>Pinus</i>	Eurythermic conifer
	Tall shrub evergreen, <i>Juniperus oxycedrus</i>	<i>Juniperus</i>	
Broadleaved tree canopy		<i>Alnus</i>	Temperate/boreal summergreen/arctic-alpine
	<i>Betula pendula</i> , <i>B. pubescens</i>	<i>Betula</i>	Boreal summergreen arctic-alpine
	<i>Corylus avellana</i>	<i>Corylus</i>	Cool-temperate summergreen
	<i>Carpinus betulus</i>	<i>Carpinus</i>	
	<i>Fagus sylvatica</i>	<i>Fagus</i>	Temperate summergreen
	<i>Fraxinus excelsior</i>	<i>Fraxinus</i>	
	Mediterranean rain green shrub		
	<i>Populus tremula</i>		Temperate/boreal summergreen
	<i>Quercus coccifera</i> , <i>Q. ilex</i>	<i>Quercus</i>	Warm-temperate broad-leaved evergreen
	<i>Quercus pubescens</i> , <i>Q. robur</i>		Temperate summergreen
	<i>Tilia cordata</i>	<i>Tilia</i>	Cool-temperate summergreen
	<i>Ulmus glabra</i>	<i>Ulmus</i>	
	Tall shrub summergreen	<i>Salix</i>	Temperate/boreal summergreen/arctic-alpine
			Warm-temperate summergreen
			Cool-temperate broad-leaved evergreen
		Warm-temperate	
		Warm-temperate sclerophyll trees/shrub	
Unforested	C3 Grass	Cereals (<i>Secale</i> excluded)/ <i>Cerealia</i> -t, <i>Secale</i> , <i>Calluna</i> , <i>Artemisia</i> , <i>Cyperaceae</i> , <i>Filipendula</i> , <i>Plantago lanceolata</i> , <i>P. montana</i> , <i>P. media</i> , <i>Poaceae</i> , <i>Rumex</i> s.p. (mainly <i>R. acetosa</i> <i>R. acetosella</i>)/ <i>R. acetosa</i> -t	Nonarboreal

* These taxa have specific pollen-morphological types; when the latter corresponds to a botanical taxon, it has the same name; if not, it is indicated by the extension "-t".

**Regional climate
model simulations for
Europe at 6 k and
0.2 kyr BP**

G. Strandberg et al.

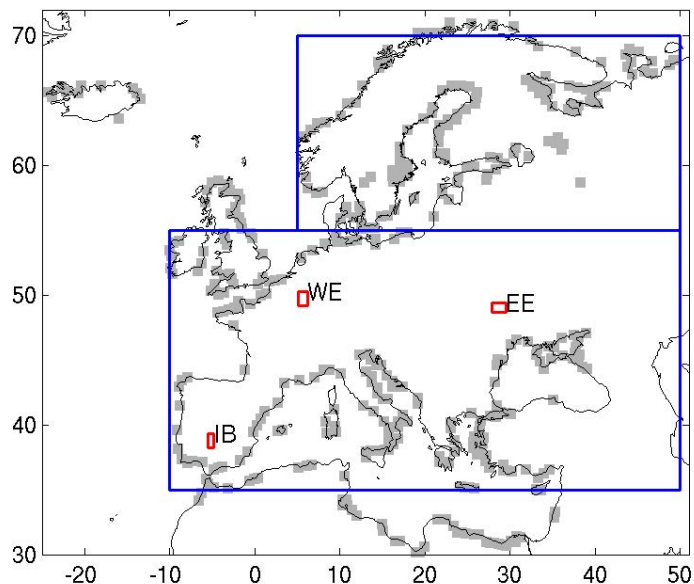


Fig. 1. Difference in land-sea distribution between 6 k and 0.2 kBP; grid boxes with a difference of more than 50 % are shaded. The three regions used for analysis in Fig. 10 are marked as red squares; Iberian Peninsula (IB), Western Europe (WE), Eastern Europe (EE). The blue boxes represent the regions Northern Europe and Southern Europe described in Sect. 4.2.

[Title Page](#)[Abstract](#)[Introduction](#)[Conclusions](#)[References](#)[Tables](#)[Figures](#)[⏪](#)[⏩](#)[◀](#)[▶](#)[Back](#)[Close](#)[Full Screen / Esc](#)[Printer-friendly Version](#)[Interactive Discussion](#)

Regional climate model simulations for Europe at 6 k and 0.2 kyr BP

G. Strandberg et al.

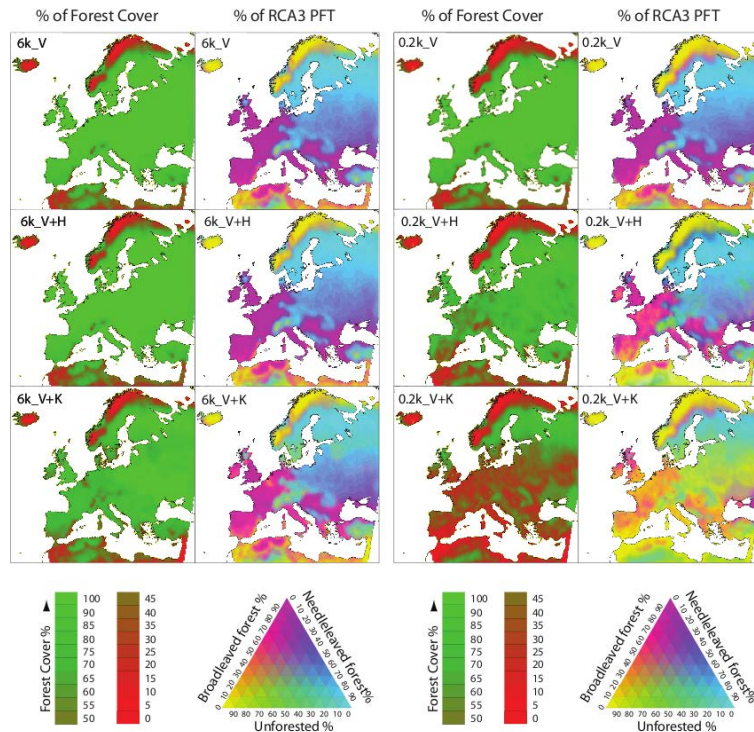


Fig. 2. Proportion of the LPJ-GUESS simulated potential natural vegetation cover (V) represented by fraction of forest (columns 1 and 3) and three RCA3 PFTs (i.e. broadleaved trees, needle-leaved trees and unforested) (columns 2 and 4) at 6 k BP (columns 1 and 2) and 0.2 k BP (columns 3 and 4). The simulation is forced by the initial RCA3 model-simulated climate. The simulated vegetation cover (V) is post-processed by overlaying the anthropogenic deforestation scenarios from the HYDE 3.1 database (Klein Goldewijk et al., 2010) (V + H) and the KK10 scenarios of Kaplan et al. (2009) (V + K). The colour scales indicates the fractions of forest and the PFTs within each grid box.

[Title Page](#)
[Abstract](#)
[Introduction](#)
[Conclusions](#)
[References](#)
[Tables](#)
[Figures](#)
[⏪](#)
[⏩](#)
[⏴](#)
[⏵](#)
[Back](#)
[Close](#)
[Full Screen / Esc](#)
[Printer-friendly Version](#)
[Interactive Discussion](#)

Regional climate model simulations for Europe at 6 k and 0.2 kyr BP

G. Strandberg et al.

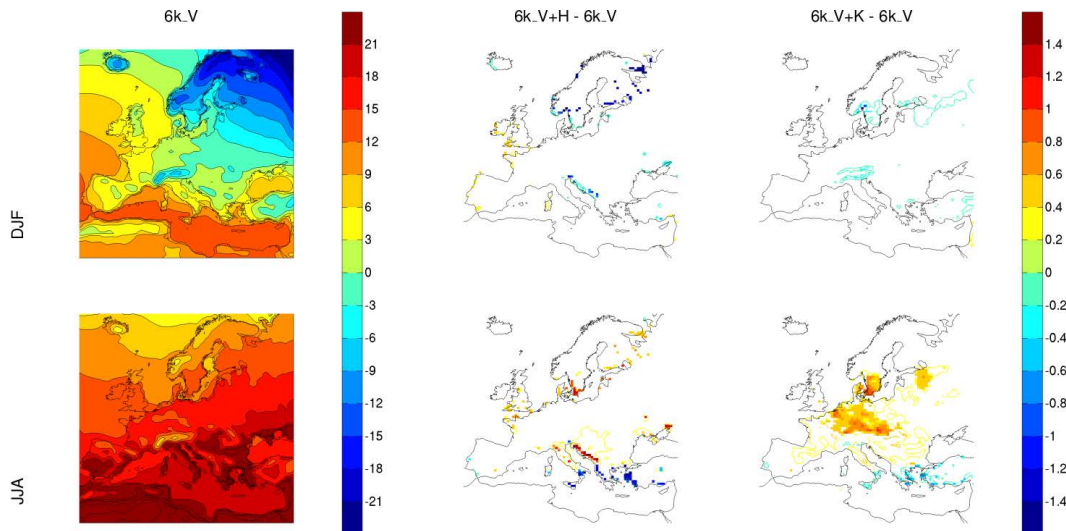


Fig. 3. Temperature ($^{\circ}\text{C}$) at 6 kBP for winter (top row) and summer (bottom row). Absolute temperature from run 6k_V (left), difference 6k_V + H – 6k_V (middle) and 6k_V + K – 6k_V (right). In the middle and right panels, grid boxes with a significant temperature difference at the 95 % level are coloured. Isolines show changes in the remaining regions. The “zero isoline” is excluded.

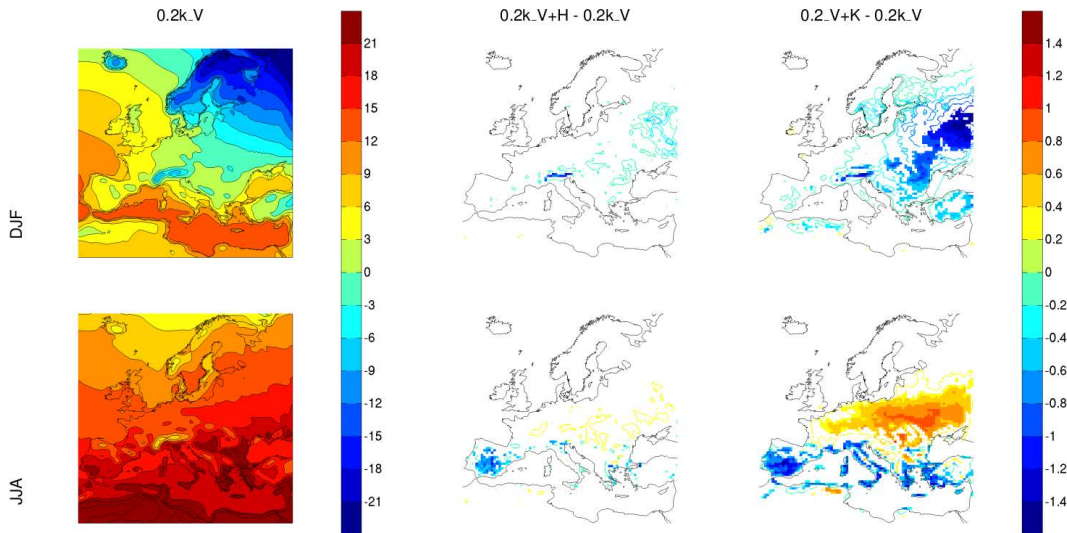


Fig. 4. Temperature ($^{\circ}\text{C}$) at 0.2 kBP for winter (top row) and summer (bottom row). Absolute temperature from run 0.2k_V (left), difference $0.2k_V + H - 0.2k_V$ (middle) and difference $0.2k_V + K - 0.2k_V$ (right). In the middle and right panels, grid boxes with a significant temperature difference at the 95% level are coloured. Isolines show changes in the remaining regions. The “zero isoline” is excluded.

Regional climate model simulations for Europe at 6 k and 0.2 kyr BP

G. Strandberg et al.

[Title Page](#)

[Abstract](#) | [Introduction](#)

[Conclusions](#) | [References](#)

[Tables](#) | [Figures](#)

[⏪](#) | [⏩](#)

[⏴](#) | [⏵](#)

[Back](#) | [Close](#)

[Full Screen / Esc](#)

[Printer-friendly Version](#)

[Interactive Discussion](#)



Regional climate model simulations for Europe at 6 k and 0.2 kyr BP

G. Strandberg et al.

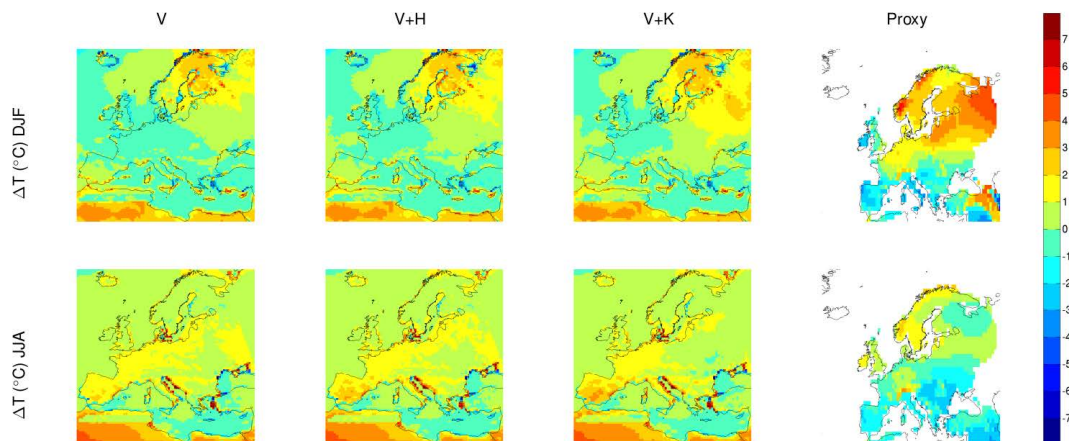


Fig. 5. Difference between RCA3 runs at 6 k and 0.2 kBP (6–0.2 k) (columns 1–3) and pollen based reconstruction (column 4) for temperature (ΔT , °C) in winter (DJF, top row) and summer (JJA, bottom row). Note that the map projection is different for the model results and proxy estimates.

Title Page

Abstract

Introduction

Conclusions

References

Tables

Figures

⏪

⏩

◀

▶

Back

Close

Full Screen / Esc

Printer-friendly Version

Interactive Discussion



Regional climate model simulations for Europe at 6 k and 0.2 kyr BP

G. Strandberg et al.

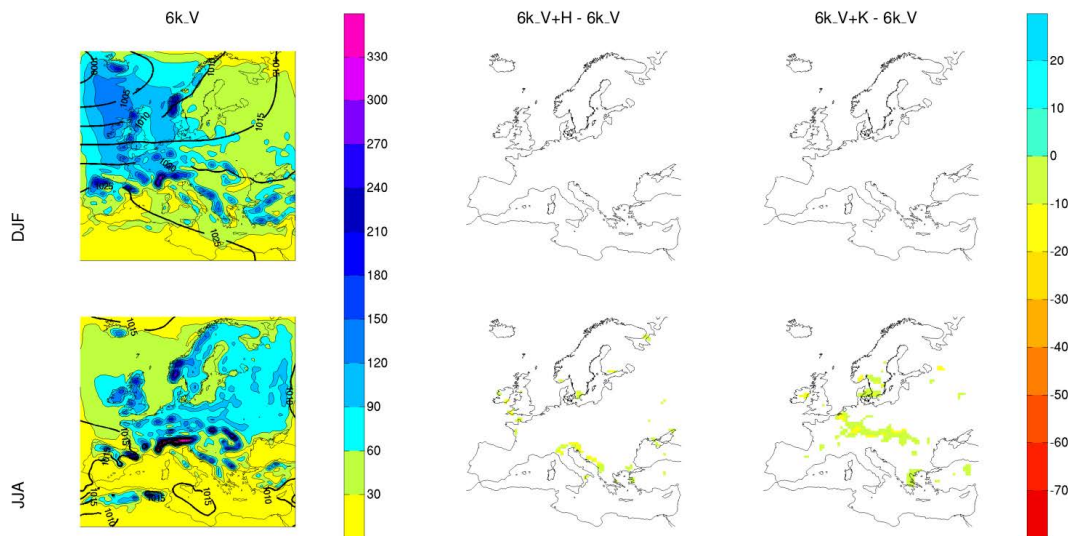


Fig. 6. Precipitation (mm month^{-1}) at 6 kBP for winter (top row) and summer (bottom row). Absolute precipitation and pressure from run 6k_V (left), difference 6k_V + H – 6k_V (middle) and difference 6k_V + K – 6k_V (right). In the left panels isolines indicate pressure (hPa). In the middle and right panels grid boxes with a significant precipitation difference at the 95 % level are coloured. Isolines show differences in the remaining regions. The “zero isoline” is excluded.

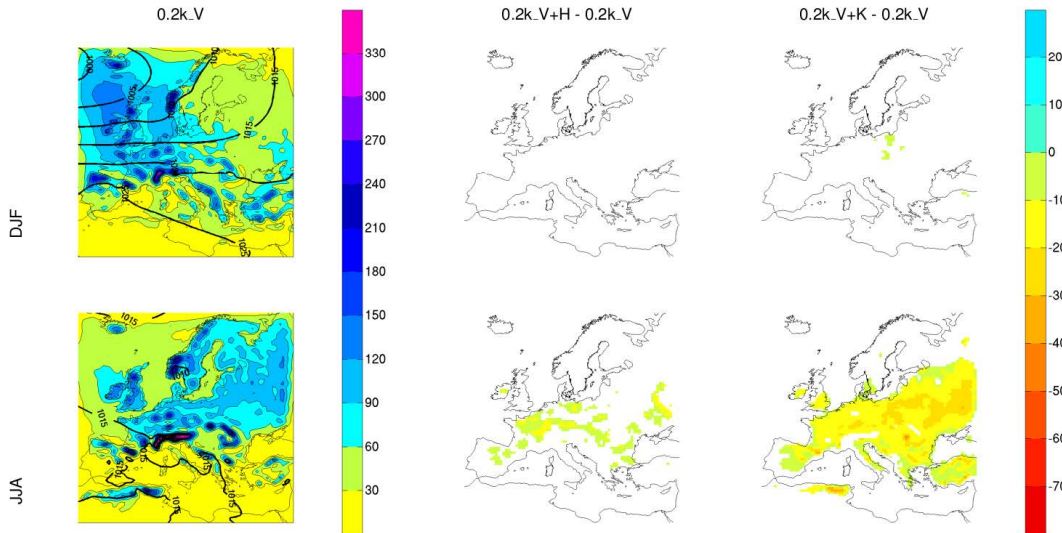


Fig. 7. Precipitation (mm month^{-1}) at 0.2 kBP for winter (top row) and summer (bottom row). Absolute precipitation and pressure from run 0.2k_V (left), difference $0.2k_V + H - 0.2k_V$ (middle) and difference $0.2k_V + K - 0.2k_V$ (right). In the left panels isolines indicate pressure (hPa). In the middle and right panels grid boxes with a significant precipitation difference at the 95% level are coloured. Isolines show differences in the remaining regions. The “zero isoline” is excluded.

Regional climate model simulations for Europe at 6 k and 0.2 kyr BP

G. Strandberg et al.

[Title Page](#)

[Abstract](#) [Introduction](#)

[Conclusions](#) [References](#)

[Tables](#) [Figures](#)

[⏪](#) [⏩](#)

[◀](#) [▶](#)

[Back](#) [Close](#)

[Full Screen / Esc](#)

[Printer-friendly Version](#)

[Interactive Discussion](#)



Regional climate model simulations for Europe at 6 k and 0.2 kyr BP

G. Strandberg et al.

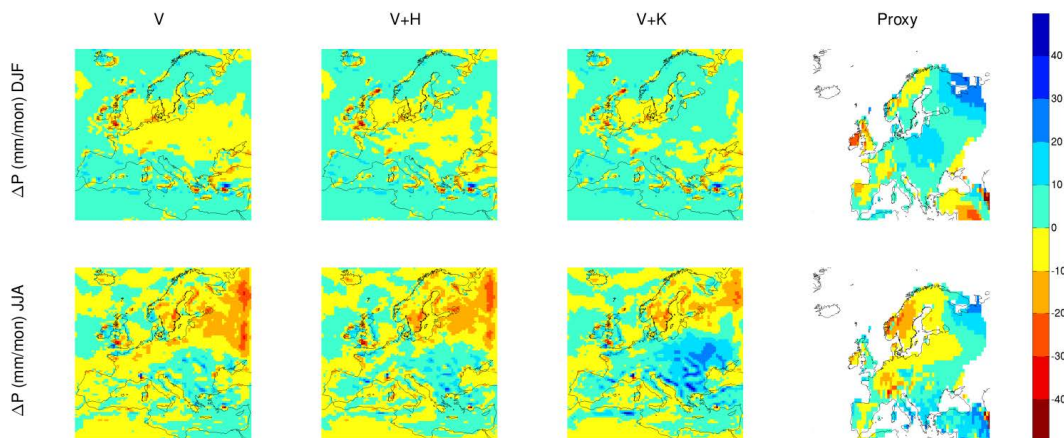


Fig. 8. Difference between RCA3 runs at 6 k and 0.2 kBP (6–0.2 k) (columns 1–3) and pollen based reconstruction (column 4) for precipitation (ΔP , mm month^{-1}) in winter (DJF, top row) and summer (JJA, bottom row). Note that the map projection is different for the model results and the proxy estimates.

[Title Page](#)

[Abstract](#)

[Introduction](#)

[Conclusions](#)

[References](#)

[Tables](#)

[Figures](#)

[⏪](#)

[⏩](#)

[◀](#)

[▶](#)

[Back](#)

[Close](#)

[Full Screen / Esc](#)

[Printer-friendly Version](#)

[Interactive Discussion](#)

Regional climate model simulations for Europe at 6 k and 0.2 kyr BP

G. Strandberg et al.

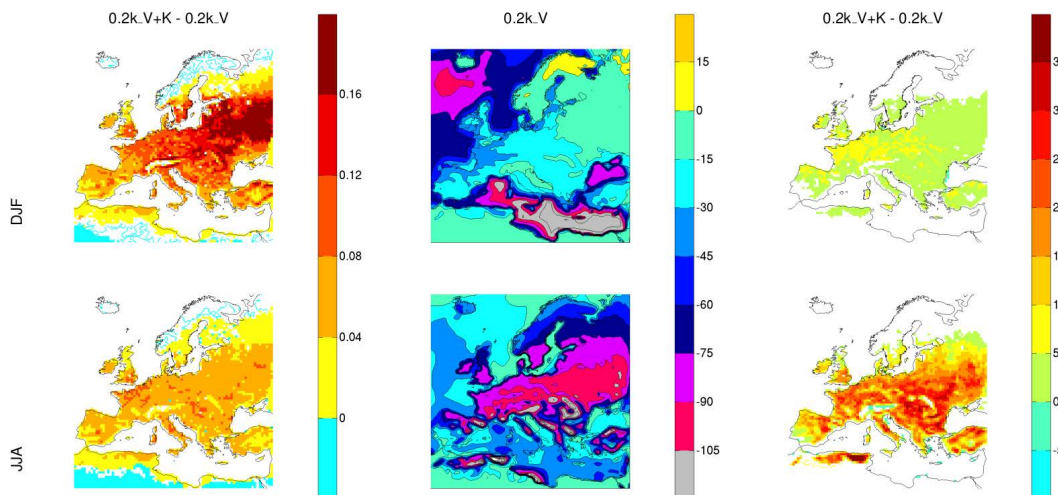


Fig. 9. Albedo difference, $0.2_V + K - 0.2_k_V$ (left), absolute latent heat flux ($W m^{-2}$) from run 0.2_k_V (middle), and difference in latent heat flux $0.2_k_V + K - 0.2_k_V$ (right) for winter (top) and summer (bottom). In the left and right panels grid boxes with a significant difference at the 95% level are coloured. Isolines show differences in the remaining regions. The “zero isoline” is excluded.

Regional climate model simulations for Europe at 6 k and 0.2 kyr BP

G. Strandberg et al.

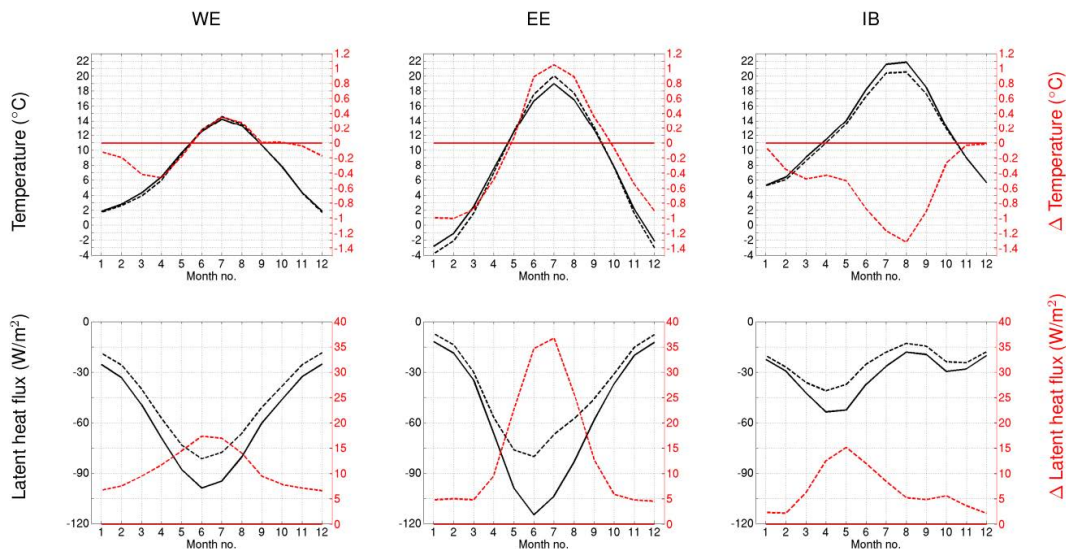


Fig. 10. Annual cycles of temperature ($^{\circ}\text{C}$, top row) and latent heat flux (W m^{-2} , bottom row) for locations in Western Europe (WE), Eastern Europe (EE) and Iberian Peninsula (IB). Black lines show absolute values and red lines show anomalies relative to 0.2 k_V. Full black line: 0.2 k_V, dashed black line: 0.2 k_V + K, full red line: 0.2 k_V – 0.2 k_V (i.e. zero difference), dashed red line: 0.2 k_V + K – 0.2 k_V. Definitions of WE, EE and IB are found in Fig. 1.

Title Page

Abstract

Introduction

Conclusions

References

Tables

Figures

⏪

⏩

◀

▶

Back

Close

Full Screen / Esc

Printer-friendly Version

Interactive Discussion

Regional climate model simulations for Europe at 6 k and 0.2 kyr BP

G. Strandberg et al.

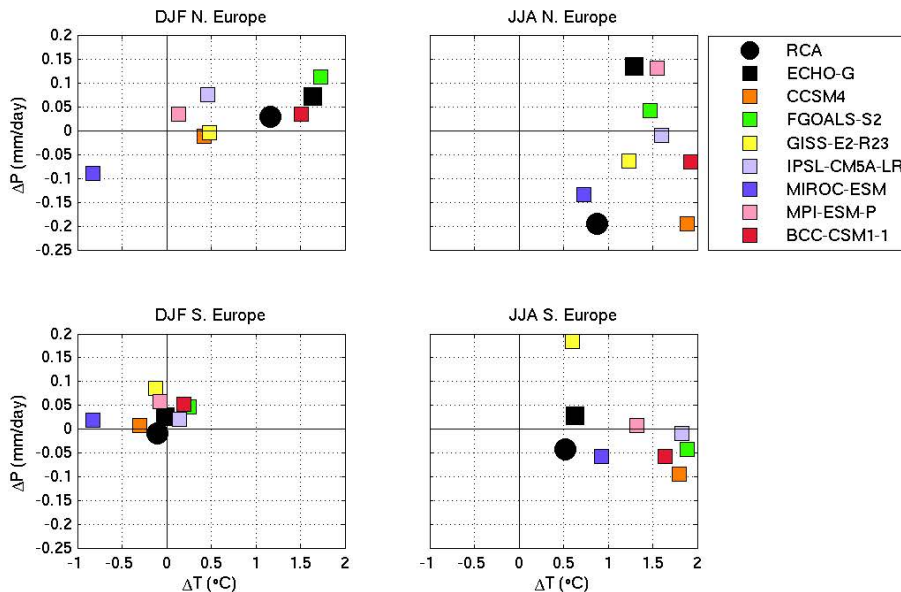


Fig. 11. Difference in temperature (ΔT) and precipitation (ΔP) between 6 kBP and 0.2 kBP in winter (left) and summer (right) in northern Europe (top) and southern Europe (bottom). The results from GCM:s are shown as coloured squares, and the result from the regional climate model RCA3 as a circle.

[Title Page](#)
[Abstract](#)
[Introduction](#)
[Conclusions](#)
[References](#)
[Tables](#)
[Figures](#)
[Back](#)
[Close](#)
[Full Screen / Esc](#)
[Printer-friendly Version](#)
[Interactive Discussion](#)

Regional climate model simulations for Europe at 6 k and 0.2 kyr BP

G. Strandberg et al.

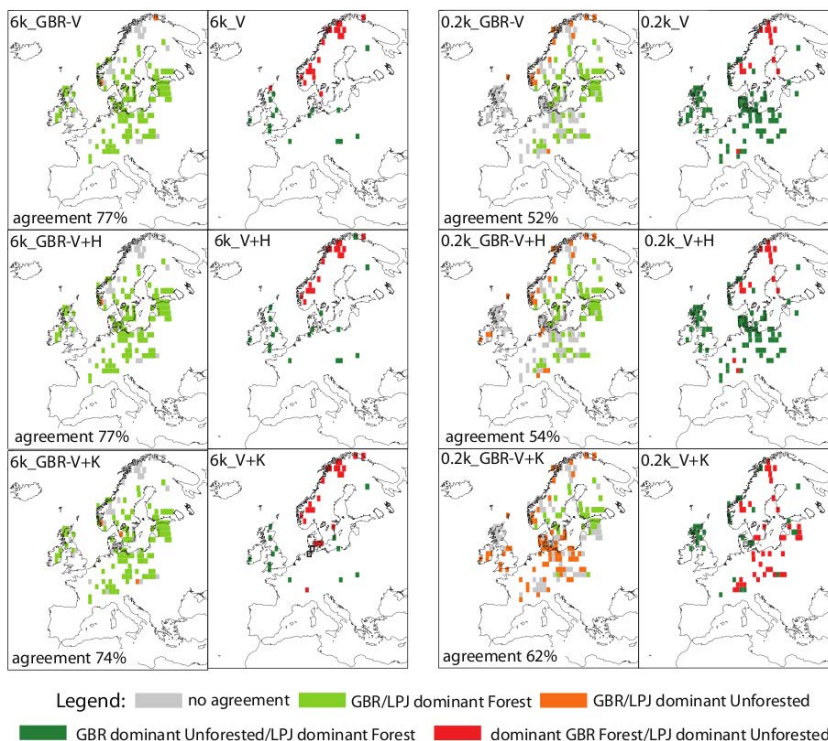


Fig. 12. Agreement (columns 1 and 3, light green or orange) and disagreement (column 1 and 3, grey; columns 2 and 4, dark green and red) between Grid-Based REVEALS (GBR) reconstructions and simulated land cover (potential natural vegetation V (upper panels), and V with the addition of two alternative anthropogenic deforestation scenarios V + H (middle panel) and V + K (bottom panel)) expressed in dominant land-cover type, i.e. > 50 % forest (light green if agreement, dark green if disagreement in GBR) or > 50 % unforested (orange if agreement, red if disagreement in GBR). Columns 1 and 2: 6 kBP; columns 3 and 4: 0.2 kBP.

[Title Page](#)
[Abstract](#)
[Introduction](#)
[Conclusions](#)
[References](#)
[Tables](#)
[Figures](#)
[Back](#)
[Close](#)
[Full Screen / Esc](#)
[Printer-friendly Version](#)
[Interactive Discussion](#)